UNIVERSITÀ DEGLI STUDI DI PADOVA

DIPARTIMENTO DI BIOLOGIA

Corso di Laurea Magistrale in Biologia Evoluzionistica

TESI DI LAUREA

Antioxidant responses in kidney of *Squalius cephalus*, chronically exposed to PFAS in rivers of Veneto region.

Relatore: Prof. Gianfranco Santovito
Dipartimento di Biologia

Correlatore: Dott.ssa Sara Pacchini
Dipartimento di Biologia

Laureando: Giacomo Vanzan

ANNO ACCADEMICO 2023/2024

INDEX

RIASSUNTO (versione italiana)

Le sostanze perfluoroalchiliche, o PFAS, sono inquinanti emergenti, riconosciuti come contaminanti ambientali onnipresenti negli ultimi anni. Diffusi in tutte le matrici ambientali, sono particolarmente presenti all'interno del sistema idrico. Sono potenzialmente in grado di causare alcune patologie; in particolare, studi precedenti dimostrano il ruolo dei PFAS nell'indurre stress ossidativo negli organismi. Il Veneto rappresenta uno dei casi più noti di contaminazione da PFAS. Nel presente studio, abbiamo valutato le risposte fisiologiche a livello del sistema antiossidante, indotte dall'esposizione ai PFAS nei corsi d'acqua della Regione Veneto. Dieci esemplari di *Squalius cephalus* sono stati campionati in tre fiumi nei pressi di Vicenza, caratterizzati da diverse concentrazioni di PFAS, ma da parametri chimici ed ecologici simili. In questo studio ci siamo concentrati sul potenziale impatto di un'esposizione cronica ad essi. Le analisi sono state effettuate nel rene, dei siti principali di bioaccumulo di PFAS e il principale organo coinvolto nell'eliminazione di queste sostanze. Un'esposizione a PFAS può quindi indurre un aumento del rischio di stress ossidativo in quest'organo. Per verificare questa ipotesi, sono stati eseguiti test di laboratorio, seguendo due diversi approcci. Abbiamo effettuato analisi molecolari per valutare i livelli di mRNA di catalasi (*cat*), glutatione perossidasi (*gpx* 1, 4), perossidredossine (*prdx* 1, 2, 3, 4, 5, 6a) e superossido dismutasi (*sod* 1, 2) attraverso qRT-PCR. E' stata analizzata l'espressione genica di isoforme differenti degli enzimi precedentemente elencati per valutare la risposta specifica in compartimenti cellulari differenti. Sono state effettuate analisi biochimiche per valutare l'attività di CAT, GPx e SOD. Sono state effettuate due analisi per valutare l'ossidazione delle proteine e dei lipidi causata dalla contaminazione da PFAS. I nostri risultati hanno mostrato una differenza dal punto di vista qualitativo delle risposte fisiologiche nel rene di *Squalius cephalus* relative alle diverse concentrazioni di PFAS. La risposta ha coinvolto diversi enzimi, attivati alternativamente in siti cellulari differenti: per esempio la CAT nei perossisomi a concentrazioni medie di PFAS e la GPx nei mitocondri e nel citoplasma ad alti livelli di PFAS. Sia basse che alte concentrazioni di PFAS determinano un aumento dell'attività di SOD, a causa di una maggiore produzione di radicale superossido. I nostri risultati mostrano un potenziale coinvolgimento degli stress granules nella risposta antiossidante nel rene. L'espressione de Prdx ha mostrato variabilità con isoforme attivate a basse concentrazioni di PFAS ed altre a livelli più elevati. In particolare, la Prdx4 è l'unica isoforma che manifesta down-regulation. I nostri dati dimostrano che una bassa contaminazione da PFAS è sufficiente per determinare un aumento dell'ossidazione delle proteine; al contrario, anche livelli elevati di PFAS non determinano un aumento della perossidazione lipidica.

ABSTRACT (English version)

Perfluoroalkyl substances, or PFAS, are emerging pollutants, recognized as ubiquitous environmental contaminants in recent years. Widespread in all environmental matrices, they are particularly present within the water system. Therefore, their toxicity represent a potential risk for all exposed organisms. They are potentially capable of causing some pathologies; in particular, previous studies demonstrate the role of PFAS in inducing oxidative stress in organisms. Veneto, an Italian region, represents one of the best-known cases of PFAS contamination. In the present study, we evaluated the physiological responses at the level of the antioxidant system, induced by PFAS exposure in watercourses of Veneto Region. Ten specimens of *Squalius cephalus* were sampled in three rivers near Vicenza, characterized by different PFAS concentration, but similar chemical and ecological parameters. The effects caused by the acute exposure to PFAS were already investigated; thus, we studied the potential impact of a chronic exposure to them. The analyses were carried out in kidney, which represents one of the principal site of PFAS bioaccumulation and the main organ involved in the elimination of these substances. Therefore, an exposure to PFAS can induce an increased risk of oxidative stress in this organ. To verify this hypothesis, laboratory tests were performed, following two different approaches. We carried out molecular analyses to evaluate the mRNA levels of catalase (*cat*), glutathione peroxidase (*gpx* 1, 4), peroxiredoxins (*prdx* 1, 2, 3, 4, 5, 6a) and superoxide dismutase (*sod* 1, 2) through qRT-PCR. Gene expression of different isoforms of the previous enzymes were analyzed to evaluate the specific response in different cellular compartments. Biochemical analyses were performed to assess the activity of CAT, GPx and SOD. Two assays were carried out to evaluate the protein and lipid oxidation caused by PFAS contamination. Our results showed a qualitative diversity of the physiological responses in the kidney of *Squalius cephalus* related to different PFAS concentrations. The response involved several enzymes, alternatively activated at different cellular sites: for example CAT in peroxisomes at medium PFAS concentrations, and GPx in mitochondria and cytoplasm at high PFAS levels. Both low and high PFAS concentrations determine an increase in SOD activity, due to a higher production of superoxide radical. Our results show a potentially involvement of stress granules in the antioxidant response in kidney. Prdxs expression showed a variable trend with isoforms activated at low PFAS concentrations and others at higher levels. In particular, Prdx4 was the only down-regulated isoform. Our data showed that low PFAS contamination is sufficient to determine an increase of protein oxidation; conversely, even high PFAS levels do not determine lipid peroxidation.

1. INTRODUCTION

1.1. THE THIRD INDUSTRIAL REVOLUTION: BETWEEN PROGRESS AND POLLUTION

In recent decades, the advent of new scientific and technological knowledge has made it possible to improve the efficiency of many industrial and agricultural activities. This new production boost contributed to coin the definition of the "third industrial revolution". While this new knowledge has increased production in different sectors, resulting in economic and social development, it has also had negative consequences. These include growing pollutant emissions into the environment, and greenhouse gases are prominent in this context. The most known CO_2, usually released by natural processes, has increased its atmospheric concentration due to anthropic activity. The leading causes of this are the use of fossil fuels in industry, transport fuels or massive deforestation. Not less important is methane CH_4; although it has a lower half-life than CO_2, it has a 70 times greater calorific value. Its concentration has increased considerably in recent decades due to intensive farming or agricultural activities, such as massive rice cultivation. In the farm sector, in recent years, the increasing use of nitrates to promote crop productivity has caused an increase in the concentration of nitrous oxide N_2O in the atmosphere. Other compounds of anthropic origin, such as pesticides in agriculture, are now present in waters worldwide. Social progress and the consequent population increase have also led to an increasing production of municipal waste, including plastics and microplastics, which now have a primary role in global water pollution.

In recent years, the interest of scientific research has shifted to the so-called "emerging contaminants", defined as chemicals or synthetic materials present in aquatic environments whose toxicity and persistence significantly affect the metabolism of a living organism (Rempel et al., 2021). These include pharmaceuticals, illicit drugs, hormones, steroids, pesticides, flame-retardants, veterinary products, food additives, perfluorochemical compounds (PFCs), bisphenol A and other substances. "Emerging pollutants" are substances released into the environment for which no legislation exists for monitoring (Thomaidis et al., 2012). In recent years, acute toxicity studies on these new pollutants have been conducted in laboratory conditions. However, the main research focus is the high persistence of these compounds in the environment. Therefore, the focus has shifted to evaluating the possible effects of chronic, prolonged exposure to these substances. The growing attention paid by research has led to an increasing monitoring of these substances in the environment and a more

restrictive regulation of their use. Ecotoxicology studies have determined the adverse effects on organisms, leading to the development of methods to remove these pollutants from the environmental matrix. However, because of their persistence in the environment, it is often difficult to trace the primary source of pollution. Among these emerging contaminants, some of the most cited compounds in recent years are PFCs; perfluorinated and polyfluorinated compounds are within this group.

1.2. THE PFAS

Per- and polyfluoroalkyl substances (PFAS) are a group of chemical surfactant compounds produced by humans since 1950 and, therefore, are not naturally present in the environment (Kissa, 2001). However, their discovery was earlier in 1938 when Roy J. Plunkett accidentally discovered polytetrafluoroethylene, later known as Teflon®. The production of these substances has increased more and more since the 1950s, having immediately assessed their remarkable properties, and their use in different industrial sectors has improved dramatically. This has led to an uncontrolled release of these substances into the water system, contaminating the aquifers over time; therefore, the water is intended for human consumption. Four thousand seven hundred thirty structures of PFAS have been recognised, 3,000 synthesised by humans; the remainder are derived from degradation or environmental transformation processes (OECD, 2018). At first, these substances did not attract scientific attention; the effects on organisms were defined as not relevant, so much to label them as "non-toxic" substances. However, the detection of these pollutants in human blood has led in recent years to the development of the first studies to assess their possible effects on the health of organisms.

1.2.1. PFAS CHEMISTRY

PFAS consist of a hydrophobic aliphatic tail composed of 4 to 16 carbon atoms in which, on one or more carbon atoms, hydrogen atoms (present in the similar non-fluorinated form from which they derive) are replaced by fluorine atoms, according to the structure -C_nF_{2n+1}- (Buck et al., 2011). They are distinguished from other PFCs by the absence of aromatic groups. The hydrophobic chain can be totally or only partially fluorinated; if fluorine atoms replace all hydrogen atoms, these substances are called perfluorinated compounds (EFSA, 2011). When only some hydrogen atoms in the aliphatic chain are replaced by fluorine atoms, they are called PFAS (Henry et al., 2018). The bond between carbon and other atoms (such as hydrogen) is subject to biotic and abiotic degradation. Therefore, PFAS would represent potential precursors of perfluoroalkyl compounds (Buck

et al., 2011). For this reason, perfluoroalkyl compounds are also referred to as terminal PFAS.

They also have a terminal hydrophilic group: a carboxyl group or a sulfonic group. PFAS are generally distinguished into long-chain molecules (PFAS-LC) and short-chain molecules (PFAS-CC). The long chain definition refers only to carboxylic perfluoroalkyl acids with at least eight carbon atoms and sulfonic perfluoroalkyl acids with at least six carbon atoms (OECD, 2018). Figure 1.1 shows an illustration of the supply chain of the high-impact PFAS.

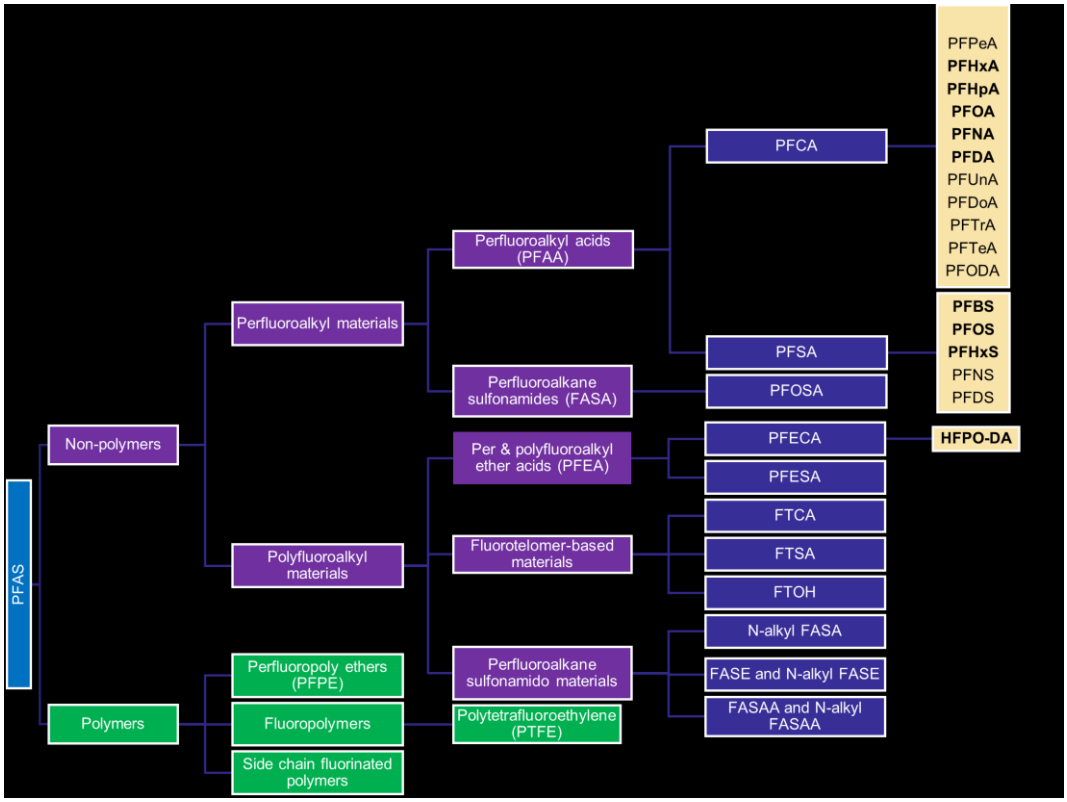

Figure 1.1. Illustration of the supply chain of the high-impact PFAS under EPA regulatory status.

Short-chain PFAS have a more hydrophilic character and tend to be more mobile in water; due to their high hydrophobicity, long-chain PFAS are less mobile in water columns but can bind to particles and, therefore, more bioaccumulative. The latter are the most dangerous for health because they are exceptionally stable and persistent in the environment and living organisms, which can be taken in through water or food (Tromba, 2017). PFAS can be solid, gaseous and liquid; most are in the form of crystalline solids or the aeriform state; the short-chain ones are generally found in the liquid state at room temperature. Furthermore, PFAS can be present as neutral, anionic, or cationic surfactants based on the charge of the terminal hydrophilic group, which depends on the pH of the environmental matrix; the most present form in the environment is anionic. These include anionic

organic surfactants, like perfluorooctanoic acid (PFOA) and perfluorooctanosulfonic acid (PFOS) (Figure 1.2). These two compounds were among the first to be detected in the environment and human blood (Bonato et al., 2020) and are known to be persistent, bioaccumulative and toxic.

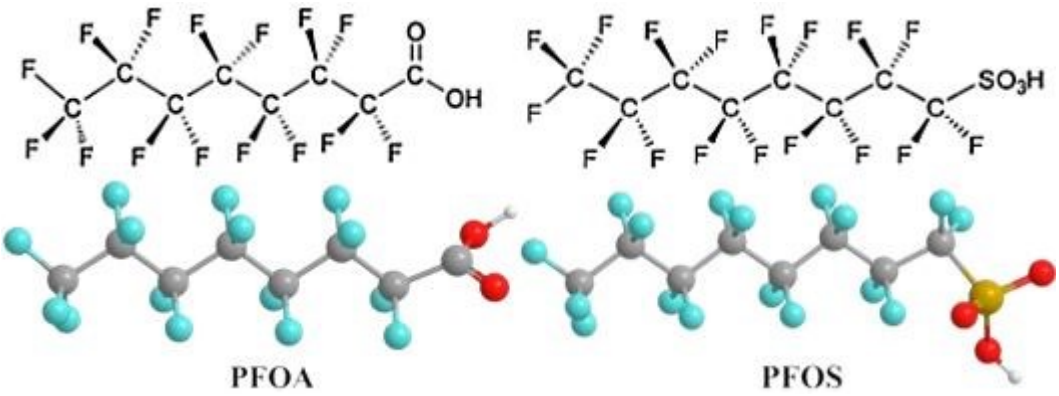

Figure 1.2. Comparison between the chemical structure of perfluorooctanoic acid (PFOA) and perluorooctanosulfonic acid (PFOS).

1.2.2. INDUSTRIAL PRODUCTION

Due to the high energy of fluoro-carbon bond formation, these compounds are not naturally found in the environment. The increasing demand in the industrial field has led to the development of different techniques aimed at their synthesis. One of the most widely used techniques until a few years ago was electrochemical fluorination, introduced in the 1940s. It consists of the electrolysis of an organic compound into a solution of hydrofluoric acid, which leads to the substitution of all hydrogen atoms for fluorine atoms. This process is inefficient, as both linear isomers are obtained, about 70%, both branched, which are the waste (Brooke et al., 2004; Prevedouros et al., 2006). Another recently introduced technique is telomerisation, which is more advantageous because it uses high-purity raw materials; therefore, equally pure products are derived with more than 99% linear isomers (EFSA, 2008). This technique consists of reacting tetrafluoroethylene with iodine pentafluoride to produce fluorotelomeres with linear alkyl chains and carbon atoms.

1.2.3. PHYSICAL-CHEMICAL PROPERTIES AND INDUSTRIAL APPLICATIONS

The variability of shapes and structures gives these compounds multiple and different chemical-physical properties. This feature determines its application in various industrial sectors. Thanks to the strength of the fluoro-carbon bonds, due to the perfect overlap of their orbitals, the PFAS enjoy remarkable chemical stability and a high thermal inertia (Kissa, 2001). This results in a high persistence of these substances in the environmental

matrix. They are resistant to oxidative degradation by atmospheric oxygen and biodegradation, photo-oxidation due to exposure to solar radiation, and hydrolysis (PFOS has an estimated half-life of more than 41 years) (Schultz et al., 2004). PFAS are poorly soluble in water and fat; therefore, they are used in the food industry, in paper processing and in the production of food packaging, which is repellent to water and oil (Lindstrom et al., 2011). They also find use in the textile industry, treating fabrics, leathers, and carpets to confer water repellence, oil repellence and stain coating (Kissa, 2001), and in agriculture as insecticides and herbicides. Fluoropolymers are also used to improve fuel delivery systems and in the oil and mining industry to increase the efficiency of oil and gas extraction (Banks et al., 1994). Also, in the home context, they are useful to give non-stick properties to pots or as surfactants and emulsifiers in detergents, polishers, waxes and paints or as cosmetics (Banks et al., 1994). PFAS enjoy a high heat resistance, guaranteed by a low boiling point, due to the limited interactions between the molecules. They are then used as flame retardants in producing foams, fire-fighting equipment (Lindstrom et al., 2011), fireproof structures, and clothing.

1.2.4. PRESENCE OF PFAS IN THE ENVIRONMENT

As a result of their increasing use, perfluoroalkyl substances (PFAS) have now been recognised as ubiquitous environmental contaminants in recent years (Brumovský et al., 2016). According to data provided by the US company 3M (the largest producer of PFOS), 26500 tonnes of waste result from the production of this substance, the majority of which is released in solid form into the environment (24500 tonnes) while the rest is dispersed in air and water (Paul et al., 2009). Regarding perfluoroalkyl carboxylic acids, 237 tonnes were emitted in 2000, 200 of which were PFOA (Prevedouros et al., 2006). However, the replacement of electrochemical fluoridation (abandoned by 3M in 2000 due to PFOS in the environment and personnel) by telomerisation has led to a significant reduction in emissions of these substances into the environment (Prevedouros et al., 2006).

Recent studies have confirmed the presence of PFAS in all the different environmental matrices, from aquatic ecosystems to sediments, flora and fauna. Therefore, it is essential to understand the soil-water distribution of PFAS to predict their mobility and biological availability in the environment and to develop remediation/management strategies (Nguyen et al., 2020). PFAS in the environment is due to inappropriate disposal of these substances, resulting in the discharge into the soil and subsequent contamination of surface water first and then aquifers. For this reason, there is higher contamination by PFAS in the most industrialised areas, near

production sites and in the most urbanised ones. Here, the most probable causes would be the discharge of industrial wastewater and fire-fighting foams used in training sites and during fire operations (Van Asselt et al., 2011). Further sources of pollution are identified in the agricultural use of fertilisers derived from urban sewage and industrial sewage sludge. Domestic and municipal waste treatment systems and the disposal of street sewage have no less impact.

However, perfluoroalkyl substances are not restricted to the most densely populated zones; they have been found far from production sites, such as glaciers and poles. In remote areas, such as the Arctic Ocean and Antarctica continent, worrying concentrations have been recorded both in predators at the apex of the food chain and at lower trophic levels, underlining the high bioaccumulation potential of these substances. PFAS in these areas would result from the degradation of their volatile precursors in the air, such as fluorotelomer alcohols (FTOH) and ethanol perfluoroottanosulfamide (FOSE), used in daily consumer products and in numerous industrial applications (Kwok et al., 2013). These compounds are much less stable but highly volatile; this allows a long-range transport and, therefore, a global diffusion, exploiting both atmospheric currents and ocean currents or marine spray (Jahnke et al., 2009; Barber et al., 2007). As a result of precipitation events, they settle on the ground or end up in surface water. Large molecules, such as phosphoric polyperfluoroalkyl esters, present in sludge from industrial wastewater treatment or used to produce waterproof food containers, release FTOH. This molecule is then converted into PFOA through biodegradation processes or chemical oxidation reactions in the atmosphere, then ending up in surface water in remote areas of the globe (Russell et al., 2008). The formation of PFOA starting from the precursor (8:2 FTOH) has also been demonstrated in vivo in rainbow trout, which was fed for seven days with fluorotelomer 8:2 FTOH, converted to PFOA through a similar process to the beta-oxidation of fatty acids (Butt et al., 2014). Therefore, when discussing airborne PFAS, we always refer to volatile precursors. To support this, in a past study, several air samples collected in different European cities were compared: the compound most found in soil was PFOA, while in the air, high levels of its precursors were detected, such as FOET, FHET, FDET (Barber et al., 2007).

Although PFAS are present in all the different environmental matrices, their largest reservoirs remain in the oceans and large water masses (Ahrens et al., 2014). In this context, reference is made to ionic PFAS (PFAA) and short-chain PFAS since they can easily be transported in water because of their relatively high polarity and solubility. Water bodies are believed to be the last global reservoir for these compounds (Prevedouros et al., 2006). To

support this, the high presence of PFOA and PFOS in ocean waters has even suggested the possibility of using these substances as chemical tracers to understand ocean circulation on a global scale better (Yamashita et al., 2008).

1.2.5. PFAS CONTAMINATION IN THE VENETO REGION

One of the most emblematic cases of PFAS contamination occurred in the Veneto region. In 2011, the Ministry of the Environment, Land and Sea commissioned a study to evaluate the contamination of Italian territory by PFAS. The study was carried out by IRSA-CNR (Water Research Institute); the results, shown in 2013, showed a high presence of PFAS in aquifers in Veneto, therefore in water intended for human consumption. High concentrations of PFOA and PFOS were recorded. This study was followed by careful monitoring by ARPAV, aimed at identifying the possible source of this contamination, subsequently identified in the Miteni company. This fluorochemical plant was considered the leading cause, even if not exclusive, and from 1964, has contributed to PFAS contamination in the Veneto waters, spreading from west to Vicenza and east to the plain of Verona and Padua (ARPAV, 2016) for a total area estimated to exceed 190 km^2 (Pitter et al. 2020). Overall, the contamination affected a total of 350˙000 citizens, exposed for over sixty years to these substances through the ingestion of contaminated food and water, mainly from the surface and well water.

Preventive measures were subsequently taken to reduce the risk of exposure to these substances. First, the Higher Institute of Health (ISS) in 2014 indicated the maximum performance values of these compounds in water intended for human consumption (PFOS <30 ng/l, PFOA<500 ng/l, sum of other PFAS <500 ng/l), sustaining that concentrations of PFBA and PFBS in waters lower than 500 ng/l didn't pose a risk to human health. In 2013, a project began in an attempt to purify water from these substances. Three barrier wells for water emulation were installed, located on the southernmost side of the Miteni plant, and a filtration system consisting of two groups of activated carbon filters. These, due to strong bonds of both physical and chemical nature, tend to retain the molecules of pollutants on the surface. Carbon filters are still periodically replaced to ensure the best water filtration. In 2017, the Veneto Region imposed new performance limits for water intended for human consumption: PFOA+PFOS < 90 ng/L, of which PFOS < 30 ng/L; the sum of other PFAS < 300 ng/L; the parameters for water intended for livestock use were kept unchanged. The Regional Council also approved, as of 2017, the second level of the "Protocol for the screening of the population of Veneto exposed to perfluoroalkyl

substances“ and the “Treatment of subjects with high concentrations of PFAS in blood”.

1.2.6. PRESENCE AND BIOACCUMULATION IN ORGANISMS

What has attracted the most research attention is the high potential for bioaccumulating these substances in organisms, including humans. In fact, high concentrations of perfluoroalkyl substances have been detected in animals at various levels of the trophic chain. In organisms, PFAS are rapidly absorbed by inhalation and ingestion and are only minimally metabolised. They have half-lives between 3,5 and 8,5 years (Cordiano and Gentilini, 2019), therefore remaining for a long time inside the body. Several studies were carried out in rats, administering radiolabelled PFOS and PFOA to demonstrate the high bioaccumulation potential of these substances in recent years. After 48 hours, only 5% of radioactive PFOS was measured in the intestines and faeces, then eliminated, suggesting that the remaining 95% had been accumulated within the body’s tissues (EFSA, 2008). Similar results were obtained for PFOA, with only 7% of the radioactivity detected in faeces (EFSA, 2008). Once absorbed by the body, PFAS, having a high affinity for proteins, can bind to serum proteins, mainly albumin (EFSA, 2008), thus being able to be distributed in different body districts. The accumulation of PFAS in the various tissues of organisms seems to be related to other factors, such as the length of the alkyl chain, the type of functional group and the protein content of the target tissue. In fact, longer-chain PFAS are more bioaccumulative than short-chain PFAS; for example, in an experiment conducted on Zebrafish in 2019, the BCF (bioconcentration factor) of PFOA (8 C atoms) was about 180 times greater than PFBA (4 C atoms) in the blood (Wen et al., 2019). Therefore, shorter-chain PFAS are less bioaccumulative and more quickly eliminated. Higher concentrations of short-chain PFAS were found in the intestines, suggesting that these substances were subsequently removed (Wen et al., 2019). Based on the functional group, experimental evidence shows that perfluoroalkyl sulfonic acids tend to accumulate more with the same number of carbon atoms than perfluoroalkyl carboxylic acids (Wen et al., 2019). Because of their high affinity for proteins, perfluoroalkyl substances accumulate more in tissues with higher protein content. Positive correlations have been found between protein concentration and PFAS accumulation (Shi et al., 2018). Therefore, the most affected organs are the liver and blood. PFAS can also cross the placental barrier, reaching the foetus (EFSA, 2008). High concentrations were also measured in the ovary in some Zebrafish studies, highlighting the possibility of being transferred to eggs, determining the possibility of developmental disorders, such as

defects in neural development, as well as embryonic mortality (Ulhaq et al., 2015).

Within organisms, these substances interfere with cellular communication and increase the risk of developing cancer. PFAS also act as endocrine disrupters, altering the proper synthesis of hormones, thereby interfering in development and reducing fertility. PFAS would also alter the correct male or female behavioural differentiation of organisms. Exposure of zebrafish individuals to increasing concentrations of PFOS is correlated with decreased expression of the brain aromatase enzyme. This protein is responsible for converting testosterone to estradiol, thus stimulating behavioural differentiation in the male sense. Therefore, exposure to PFOS would be related to a plausible behavioural differentiation in the female sense (Shi et al., 2008). In a 2019 study, exposure to PFAS resulted in males increasing expression of VTG (typically expressed in females), related to an alteration in the testosterone/estradiol ratio, suggesting estrogenic-like activity of these compounds.

1.3. ROS: REACTIVE OXYGEN SPECIES

Oxygen O_2 represents the fundamental molecule for the life of all aerobic organisms. In fact, at the mitochondrial level, it is used as the final acceptor in the electron transport chain (ETC) during the oxidative phosphorylation aimed at the synthesis of ATP. During this process, the high-energy intermediates generated by the macronutrient catabolism undergo oxide-reductive (redox) reactions to create the electrons' flow. These are translocated by mobile electron transporters, such as ubiquinone (or coenzyme Q) and cytochrome c (cyt c). Electron transfer is coupled to proton transfer from matrix to intermembrane space, generating an electrochemical gradient to push ATP synthase to produce ATP (Ghifari et al., 2023). At the end of this process, the electrons are transferred to the oxygen, which undergoes a tetraelectronic reduction by the cytochrome oxidase, forming water.

$$O_2 + e^- \rightarrow \bullet O_2^- + e^- \rightarrow H_2O_2 + e^- \rightarrow \bullet OH + e^- \rightarrow H_2O$$

However, this chain can be interrupted at various levels. Therefore, during electron transfer reactions, partially reduced byproducts of oxygen metabolism may be formed: it has been calculated that 3% of the O2 used by cells is improperly converted into undesirable intermediates, called ROS (Santovito et al., 2005). Some studies on experimental mammals verified that more than 90% of the ROS are generated in mitochondria, and approximately 2% of the whole O_2 uptake is accounted by ROS generated as obligatory byproducts of oxidative metabolism (Wilhelm Filho, 2007). The first definition of reactive oxygen species, or ROS, was proposed by

Danharm Harman in 1956, who called them "chemical species, chemically reactive, containing oxygen". ROS are divided into radical and non-radical species. The firsts contain at least one unpaired electron in the outermost orbital, which gives them high reactivity (Jomova et al., 2023). They include, among others, the superoxide anion ($\bullet O_2^-$), the hydroxyl radical ($\bullet OH$), alcoxyl radicals, peroxylic radicals ($\bullet ROO^-$) and the hydroperoxide radical. Non-radical species do not have unpaired electrons in the outermost orbital and mainly include hydrogen peroxide (H_2O_2), singlet oxygen, ozone and lipid peroxides.

ROS at physiological concentrations play a fundamental role in regulating multiple biological processes, such as cell proliferation, differentiation, apoptosis, migration and necrosis. In fact, they are essential for maintaining the correct physiological functions, redox balance and regulation of transcription factors (Jomova et al., 2023). For example, they regulate the expression of NF-kB transcription factor, which influences the transcription of genes involved in immune response and inflammatory states. They act directly by changing the expression of the Nrf2 factor that activates genes responsible for the antioxidant response. However, high concentrations of ROS can cause an imbalance in the redox equilibrium, resulting in a state of oxidative stress with damage to macromolecules such as DNA, proteins and membranes (Liguori et al., 2018). Therefore, the concentration of ROS is kept within a homeostatic range. Oxidative stress is the breakdown of the balance between forming and eliminating free oxygen radicals (Figure. 1.3).

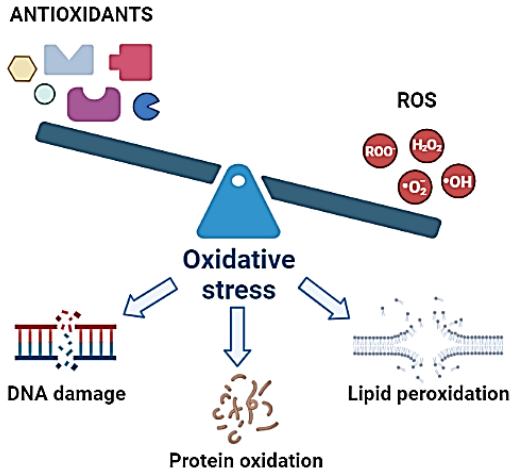

Figure 1.3. Balance between forming and eliminating ROS.

Because of their unstable nature, ROS tend to "sequester" electrons from other macromolecules, generating new radical species. In particular, they can oxidise proteins, changing their amino acid structure and thus alternating their function. They can involve the inactivation of enzymes, interfere with intracellular signalling pathways and determine the

degradation of proteins. ROS can act directly on DNA, inducing mutations and potentially contributing to the development of various pathologies, such as cancer. They can react with membrane lipids, initiating a chain reaction known as lipid peroxidation, thus compromising the integrity of membranes potentially leading to premature death of the cell. A high production of ROS can also lead to mitochondrial damage. The cumulative effects of ROS ultimately determine the development of different pathological states: in addition to the already mentioned cancer, cardiovascular diseases, diabetes, neurological disorders (Alzheimer's and Parkinson's disease, Down syndrome), psychiatric diseases (depression, schizophrenia, bipolar disorder), kidney disease, lung disease (chronic pulmonary obstructions, lung cancer) and ageing (Jomova et al., 2023).

Multiple factors participate in the formation of ROS. Environmental changes can increase or decrease oxygen availability, resulting in an accentuated risk of oxidative stress. In the aquatic environment, the solubility of oxygen is inversely proportional to temperature and salinity and directly proportional to pressure. Therefore, an increase in temperature results in a decrease in the solubility of oxygen, which becomes less available to organisms, entering a state of hypoxia; instead, the opposite condition leads the organisms to a state of hyperoxia. In both situations, a variation in the partial pressure of oxygen determines the increase in the formation of ROS and, consequently, an enhanced risk of oxidative stress.

Endogenous, exogenous and pathological causes are distinguished in the formation of ROS. Among the endogenous sources are all those reactions that occur within the body, which can mistakenly lead to the production of ROS. Mitochondria, particularly the ETC, is the most responsible site for the production of ROS in proportion to the stress state of the cell. The loss of some electrons from the ETC can determine the formation of the $\bullet O_2^-$. Other endogenous sources are represented by several enzymes typically involved in physiological processes, such as NADPH oxidase, xanthine oxidoreductase and cytochrome p450. The latter is involved in various metabolic pathways, including the metabolism of drugs, environmental pollutants and other xenobiotics, the biosynthesis of steroid hormones, and the oxidation of unsaturated fatty acids in intracellular messengers and fat-soluble vitamins (Hasler et al., 1999). Under conditions of potential stress, such as exposure to contaminants, cytochrome P450 can lead to the development of ROS. The inflammatory state represents an additional endogenous source: immune system cells such as neutrophils and macrophages produce ROS as a defence mechanism against pathogenic organisms. The endoplasmic reticulum is the cell compartment responsible for maintaining calcium homeostasis; in conditions of imbalance of calcium

ion levels, the ER can lead to the accumulation of ROS. Free radicals are also formed through non-enzymatic reactions involving metal ions like iron and copper. In particular, the reactions of Fenton and Haber-Weiss lead to •OH formation. Another significant source is peroxisomes; these organelles are involved in various metabolic processes, such as the oxidation of fatty acids and the metabolism of ROS, particularly H_2O_2.

Exogenous sources of ROS include factors external to the body, such as ionising radiation, excessive use of drugs, smoking, alcohol consumption, ultraviolet radiation, exposure to environmental contaminants and xenobiotics, chemotherapy and radiation therapy. Smoking is a significant source of ROS, damaging the gastrointestinal tract. It has been proved that cigarette smoke contains high concentrations of various compounds (oxidants and free radicals) involved in the initiation and promotion of oxidative damage, which leads to various degenerative pulmonary, cardiovascular diseases and cancer (Mureşan et al., 2008). High consumption of red meat is correlated with increased oxidative stress. Red meat contains a high iron content that can catalyse the formation of ROS in the colon during digestion (Valko et al., 2001).

The pathological sources refer to ROS production due to diseases. Some examples are immune cell activation, inflammation, cardiovascular diseases, ischemia, infections, cancer, metabolism of environmental pollutants and certain drugs. Therefore, when produced in excess, ROS can cause tissue injury. However, tissue injury can itself cause ROS generation (e.g., by causing activation of phagocytes or releasing transition metal ions from damaged cells), which may (or may not, depending on the situation) contribute to a worsening of the injury (Aruoma, 1998).

1.3.1. SUPEROXIDE ANION (•O_2^-)

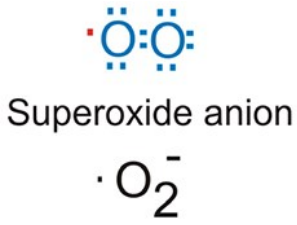

Figure 1.4. Lewis's formula and chemical formula of superoxide anion.

The •O_2^- (Figure 1.4) is the first intermediate in the ETC. For this reason, it is called primary ROS (Valko et al., 2004). It results from the monoelectron reduction of molecular oxygen (Sikora et al., 2017) mediated enzymatically by NADPH oxidase and xanthine oxidase or in a non-enzymatic way by redox compounds, such as ubiquinone. In vivo, it is produced in the mitochondrion ETC complex I and III. Within the cell, it can react with other

reduced substances or macromolecules. However, the $\bullet O_2^-$ exhibits relatively low reactivity with biological molecules (Jomova et al., 2023) and has a reduced half-life (Sikora et al., 2017). It can react with metal ions such as copper or iron by generating the •OH through the Fenton reaction or with the superoxide dismutase (SOD) that reduces it to H_2O_2.

1.3.2. HYDROGEN PEROXIDE (H_2O_2)

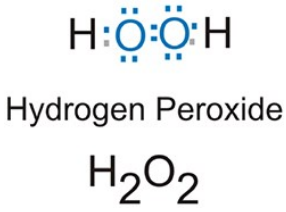

Figure 1.5. Lewis's formula and chemical formula of hydrogen peroxide.

H_2O_2 (Figure 1.5) is derived from the dielectronic reduction of molecular oxygen. A non-radical character, compared to other ROS, it represents the least dangerous form. Under physiological conditions, it is produced inside the peroxisomes, where the numerous proton pumps near the plasma membrane allow hydrogen to be transferred inside the organelle, forming H_2O_2. The dismutase reaction by SOD mostly produces it, but it can also be formed by the dielectronic reduction of oxygen by oxidases, such as xanthine oxidase or glucose oxidase (Jomova et al., 2023). As mentioned above, H_2O_2 is usually produced by the body and is involved in the inflammatory response to eliminate pathogenic organisms and in different intracellular communication pathways.

1.3.3. HYDROXYL RADICAL (•OH)

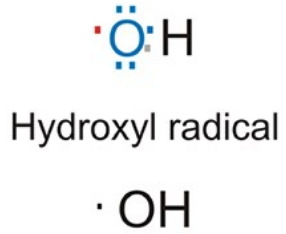

Figure 1.6. Lewis's formula and chemical formula of hydroxyl radical.

The •OH (Figure 1.6) derives from the trielectronic reduction of molecular oxygen, representing the third reactive oxygen intermediate. Among ROS, it is the most reactive form and, thus, the most dangerous, also because no antioxidant enzyme can eliminate it specifically. Therefore, the best solution to prevent damage caused by the •OH is to limit its formation to the formation of its precursors. This ROS can be formed from $\bullet O_2^-$ and H_2O_2 through the Haber-Weiss reaction:

$$\bullet O_2^- + H_2O_2 \rightarrow \bullet OH + OH^- + O_2$$

The •OH can also form from hydrogen peroxide alone through the Fenton reaction:

$$Fe^{2+} + H_2O_2 \rightarrow Fe^{3+} + \bullet OH + OH^-$$

1.3.4. SINGLET OXYGEN ($^*O_2$)

Singlet oxygen, like H_2O_2, does not contain unpaired electrons in the outermost orbital, representing a reactive diamagnetic species (Jomova et al., 2023). Singlet oxygen is an exceptionally reactive species and can interact with different biological molecules; however, it tends to interact more with the double bonds of polyunsaturated fatty acids.

1.3.5. PEROXYLIC RADICAL (ROO•) AND LIPID PEROXIDATION

The peroxyl radical (ROO•) is an exceptionally reactive species found within organisms due to the interaction of ROS with hydrocarbon chains. Within organisms, when we talk about ROO•, we often refer to peroxylic radicals that form near biological membranes. In the presence of oxidative stress, the interaction of reactive species such as $\bullet O_2^-$ or •OH with membrane lipids determines the formation of ROO•. These can react with other adjacent membrane lipids, promoting the formation of lipid radicals and lipid peroxyl radicals. The formation of lipid peroxyl radicals is hazardous for the cell, as the unpaired electron can transfer from one phospholipid to another in a chain reaction called lipid peroxidation. The oxidised phospholipid does not return to normal but remains permanently damaged. Therefore, the formation of lipid peroxyl radicals causes damage that expands very quickly at the level of the biological membranes, causing alterations in the structure and cellular functions until the cell's death.

1.4. OXIDATIVE STRESS INDUCED BY PFAS IN THE KIDNEY

Previous studies have shown that the kidneys may be one of the main sites of accumulation of PFAS in aquatic organisms. For example, in exposure studies on *Oncorhynchus mykiss,* higher PFC concentrations were found in the blood, followed by the kidneys and liver (Savoca and Pace, 2021). Moreover, the kidney is particularly susceptible to oxidative stress for many anatomical and physiological reasons. The kidney is particularly prone to hypoxia, especially in kidney disease conditions or reduced blood perfusion, resulting in increased ROS. The kidney also detoxifies toxic molecules using an active transport mechanism. Therefore, exposure to xenobiotics, such as PFAS, may lead to increased renal activity aimed at eliminating these substances. Renal elimination of PFAS includes a passive diffusion process, namely glomerular filtration, and two active pathways, namely tubular secretion and resorption (Figure 1.7). Secretion and reabsorption of PFAS in the kidney are mediated by renal transporters

expressed on the basolateral (opposite blood) and apical (opposite urine) membranes of proximal tubular cells (Niu et al., 2023). The currently known PFAS renal transporters are members of two transporters families: the SLC and ABC superfamilies. SLC transporters non require the ATP hydrolysis, while ABC transporters are ubiquitous membrane proteins that use ATP hydrolysis and mostly function as efflux transporters (Niu et al., 2023). This increase in activity, due by PFAS exposure, is followed by an increase in ROS and a subsequent alteration of the antioxidant response in the kidney to limit the risk of oxidative stress.

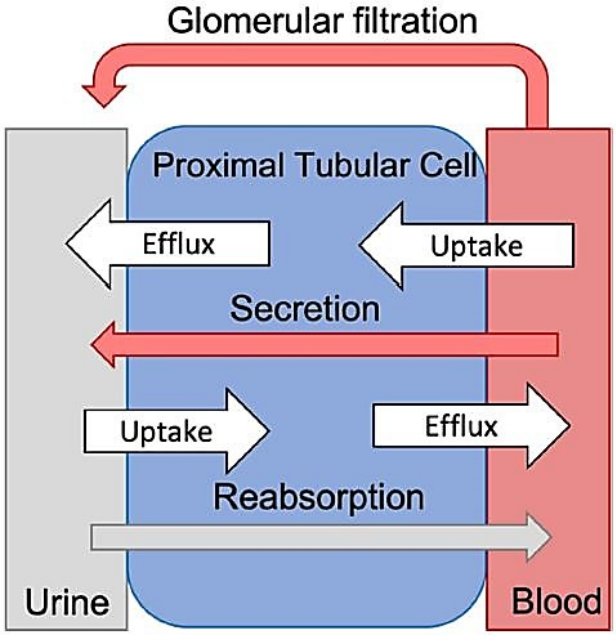

Figure 1.7. Mechanism of secretion and reabsorption of PFAS in the kidney.

1.5. ANTIOXIDANT DEFENCES

The cells, subjected to a higher partial pressure of oxygen, are therefore potentially exposed to the attack of ROS; for this reason, the organisms have evolved a sophisticated system of antioxidant defences aimed at balancing the concentration of ROS and minimising their damage. Antioxidant defences include antioxidant enzymes and low molecular weight non-enzymatic molecules (Figure 1.8). The latter are nucleophilic and reducing molecules capable of reacting with oxidants, generally electrophiles, giving them one or two electrons (Espinosa-Diez et al., 2015). In this way, they can inhibit or stop the oxidation reaction to the damage of other molecules.

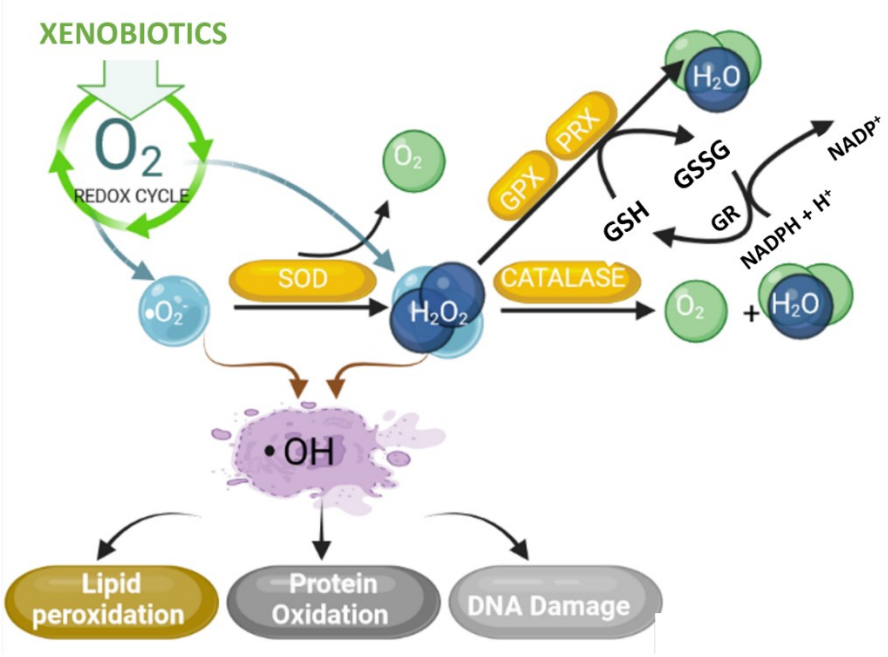

Figure 1.8. Representation of production and detoxification of different ROS by non-enzymatic and enzymatic defences.

1.5.1. NON-ENZYMATIC ANTIOXIDANT DEFENCES

The non-enzymatic antioxidant defences include both endogenous molecules, synthesised directly by the body, and exogenous ones, which must be assimilated with the diet. The firsts include glutathione (GSH) and metallothioneins (MT).

MT are a family of low molecular weight, ubiquitous, monomeric, cytoplasmic proteins with a gene counterpart that, when activated, allows its biosynthesis. Being very rich in cysteine residues that coordinate zinc atoms, they can bind metals with different affinities, thus protecting the cell from excess metals. In addition, the zinc ion, released following the binding of MT with other metals, activates other transcription factors, which in turn activate the transcription of antioxidant enzymes through the bond with the Metal Response Elements. They also have direct antioxidant action, acting as scavengers against ROS: the thiol groups of cysteines can react with ROS, oxidising and forming disulfide bonds.

GSH is considered the most abundant molecule among endogenous antioxidants. It consists of a tripeptide composed of glutamate, cysteine and glycine. Unlike MT, it is not encoded by a gene but biosynthesised by the enzymes γ-glutamate *cysteine ligase* and glutathione synthetase. GSH can donate an electron to the ROS, oxidising itself and then forming a disulfide bridge with another molecule of oxidised glutathione, generating the dimer GSSG. Therefore, it can act directly as a scavenger against reactive oxygen molecules. It is also used as an indispensable reducing factor for the

functioning of antioxidant enzymes, such as glutathione peroxidase (GPx) or peroxiredoxins (Prdx) or as a cofactor from glutathione S-transferase (GST). To keep the GSH/GSSG ratio constant, GSSG is moved out of the cell and degraded in the extracellular environment, or it can be enzymatically reduced again by the action of glutathione reductase (GR).

Animals cannot biosynthesise exogenous antioxidants and can only be assimilated through the diet. This group includes ACE vitamins, carotenoids (β-carotene and xanthophyll), polyphenols and certain minerals. Carotenes and xanthophylls are lipophilic substances contained in fruits and vegetables; they interrupt the chain reactions of peroxylic radicals, thus acting as chain breakers and can act as singlet oxygen quenchers. Vitamin E, or tocopherol, a powerful lipophilic antioxidant, acts as a radical chain breaker and scavenger of ROS. Vitamin C is a hydrophilic antioxidant; it acts as a digger against several ROS and helps reduce the tocopheryl radical, regenerating tocopherol.

1.5.2. ENZYMATIC ANTIOXIDANT DEFENCES

Unlike non-enzymatic antioxidant molecules, antioxidant enzymes can eliminate ROS through continuous reactions over time. Non-enzymatic antioxidants remain permanently damaged by the reaction with ROS; only in some cases, the oxidation is reversible, as in the case of tocopherol. Antioxidant enzymes, on the other hand, reduce ROS by oxidising themselves; however, later, they are reduced again by other molecules, which act as reducing factors. In this way, antioxidant enzymes become available again to react with other ROS. Antioxidant enzymes are a class of proteins that catalyse the transformation of ROS or their byproducts into more stable, usually less harmful, species (Jomova et al., 2023). Some enzymes can act synergistically in the defence action against ROS (Krishnamurthy and Wadhwani, 2012), rendering the system very complex. Antioxidant enzymes include mainly SOD, GPx, catalase (CAT), and Prdx. To these are also added thioredoxin reductase (TrxR), glutathione reductase (GR), as well as the same enzymes responsible for the biosynthesis of GSH (γ-glutamate *cysteine ligase* and glutathione synthetase).

1.5.2.1. SUPEROXIDE DISMUTASE (SOD)

Figure 1.9. Crystal structure of Cu/Zn superoxide dismutase.

SOD (Figure 1.9), belonging to the class of oxidoreductases, is a multigenic family of metalloproteins present in the cells of all organisms. The first SOD studied was extracted from bovine erythrocytes (Stephenie et al., 2020). They are dimeric or tetrameric proteins containing a metal cofactor within the active site, responsible for the enzyme's catalytic activity. The cofactor can donate an electron to ROS, reducing them. The catalytic function of SOD was discovered in 1969 (McCord and Fridovich, 1969). They catalyse the dismutation reaction of the $\bullet O_2^-$ to molecular oxygen and H_2O_2 in two steps:

$$\textbf{E-me (ox)} + \bullet O_2^- \rightarrow \textbf{E-me (red)} + O_2$$

$$\textbf{E-me (red)} + \bullet O_2^- + 2H^+ \rightarrow \textbf{E-me (ox)} + H_2O_2$$

In the first reaction, the oxidised metal cofactor at the active site reacts with the $\bullet O_2^-$, reducing itself and catalysing the formation of molecular oxygen. In the second reaction, the metal cofactor, now reduced, reacts with a second $\bullet O_2^-$ molecule; this determines the return to the oxidised state of the heme group and the formation of an H_2O_2 molecule. SOD eliminate two molecules of $\bullet O_2^-$, producing oxygen and H_2O_2.

1.5.2.1.1. SODs ISOFORMS

Four isoforms of SODs are known, characterised by the presence of different metals in their active site: copper-zinc, manganese, iron, and nickel.

- **Cu/Zn-SOD**

  Together with manganese SOD, copper-zinc SOD is the most common isoform in animals. First isolated in 1938 by Mann and Keilin, it is present in eukaryotes in two isoforms: an intracellular, encoded by the *sod1* gene and an extracellular, EC-SOD, encoded by the *sod3* gene. SOD1 is a homodimeric protein (32 kDa) located in eukaryotic cytoplasm, chloroplasts and some prokaryotes. Each monomer has a barrel structure of eight antiparallel-β-leaflets. EC-SOD is a homotetrameric glycoprotein composed of two dimers joined through a disulphide bridge (Poli et al., 2018). It is a secretion protein localised in the extracellular matrix at the level of the interstitial fluid or anchored to the plasma membrane. Compared to other isoforms, SOD1 and SOD3 coordinate two different metal ions in the active site; however, only the copper ion participates in catalytic activity, while the zinc ion only has a structural function, giving structural stability and electrostatic stabilisation (Kumar et al., 2022). The active site contains some highly conserved amino acid residues during evolution, which can coordinate the two metal ions. In particular, the zinc ion is coordinated by His^{45},

His^{47}, His^{62} and His^{119}, while His^{62}, His^{70}, His^{79} and Asp^{82} coordinate the copper ion. The remnant His^{62} forms a bridge between the two ions (Kumar et al., 2022). A threonine and an arginine drive the $\bullet O_2^-$ to the copper ion within the active site.

- **Mn-SOD**

Manganese SOD is a homotetrameric enzyme of about 96 kDa. The *sod2* gene encodes it. It consists of four identical subunits, each containing one Mn^{3+} atom, and it is present in prokaryotes and within the mitochondrial matrix of eukaryotes. Each monomer has two distinct domains: an N-terminal helical hairpin domain and a C-terminal domain, containing five α-helixes and three antiparallel-β-sheets (Candas and Jian Li, 2014). Some residues are highly conserved during evolution: in particular, the residues Asp^{159}, His^{163}, His^{26}, and His^{74}, associated with a water molecule for each subunit, coordinate the manganese atom within the active site (Candas and Jian Li, 2014). Mn-SOD is the primary antioxidant defence at the mitochondrial level, the site of the highest production of ROS, due to the ETC. Therefore, it is an essential and biologically significant molecule for aerobic cells. Previous studies have shown that the *sod2* gene knockout is lethal in mice and fruit flies (Williams et al., 1998). Heterozygous mice with reduced Mn-SOD activity exhibit more oxidative stress. Using E. coli, the importance of Mn-SOD expression for survival in aerobic environments has been demonstrated (Gregory and Fridovich, 1973).

- **Fe-SOD**

Iron SOD is a dimeric (40 kDa) or tetrameric protein containing three histidines and an aspartic acid that stabilise the iron atom bond within the enzyme's active site (Stephenie et al., 2020). Present in prokaryotes, protozoa and chloroplasts, it is classified as chelating due to multiple donor groups of atoms capable of attaching a metal ion (Jamdhade et al., 2017). The Fe-SOD isoform of plants can contribute as a potential mediator of elimination of free radicals due to its ability to retain multiple donors of atoms (Stephenie et al., 2020).

- **Ni-SOD**

Discovered in 1996 in the genus *Streptomyces*, Ni-SOD was a real surprise for the scientific community, as Ni(II) represents the only stable oxidation state in aqueous media and cannot catalyse the dismutation of $\bullet O_2^-$ in aqueous solution. The adaptations required to use this metal as a catalytic centre determined the unique evolution of this enzyme that does not exhibit sequence homology with other SOD. Ni-SOD is

commonly found in cyanobacteria, which were the first to produce oxygen, and is also present in some marine eukaryotes, making it the most abundant SOD in modern oceans (Alfano and Cavazza, 2020). It is a small homotetrameric protein; each subunit contains about 117-120 amino acids (Poli et al., 2018).

1.5.2.2. GLUTATHIONE PEROXIDASE (GPx)

Figure 1.10. Crystal structure of glutathione peroxidase 4.

GPxs (Figure 1.10) are a multigenic family of metalloproteins that catalyse the reduction of H_2O_2 or organic hydroperoxides by water or in the corresponding hydroxyl compounds, using reduced glutathione GSH as an electron donor (Margis et al., 2008), through a divalent reduction.

$$\mathbf{2GSH + H_2O_2 \rightarrow GSSG + 2H_2O}$$

$$\mathbf{2GSH + R\text{-}OOH \rightarrow GSSG + R\text{-}OH}$$

They are homotetrameric or monomeric proteins; each subunit consists of seven β-sheets and four α-helices. Eight isoforms have been characterised in mammals, with different subcellular localisations. In particular, GPx-1, GPx-2, GPx-3, GPx-4, and GPx-6 (in some species) are termed selenium-dependent for the exclusive presence of selenocysteine; GPx-5, GPx-7, and GPx-8 are termed non-selenium-dependent. Selenium-dependent GPxs can detoxify organic and inorganic peroxides; non-selenium-dependent GPxs can only reduce organic ones. They are all characterised by a highly conserved catalytic tetrad formed by cysteine (or selenocysteine), glutamine, tryptophan and asparagine.

Selenocysteine is encoded by the codon TGA, which usually acts as a stop codon, causing the interruption of translation. How the selenocysteine residue was incorporated into the protein remained an enigma for a few

years, and was eventually discovered for serendipity. In 1986, by examining the cDNA of mouse erythroblasts, for which the relevant protein was not yet known, it was found to encode for a bovine GPx1 homologue that had been sequenced in the meantime. Surprisingly, the stop codon TGA was noted in the position of selenocysteine in the bovine GPx1, concluding that TGA could somehow encode selenocysteine. A further study of the same year showed the stop codon TGA in the position of selenocysteine within bacterial dehydrogenase. With the increasing number of DNA and peptide sequences, it became evident that the TGA codon was generally used by nature to encode selenocysteine (Flohé et al., 2022). The insertion of selenocysteine into the peptide chain requires the intervention of a special Sec-tRNA and the presence in the '3' UTR region of the mRNA of a selenocysteine insertion sequence consisting of a series of nucleotides that form a stem-loop region. Recognising the TGA codon as a site for incorporating selenocysteine rather than as a stop codon involves the SBP2 factor binding to the stem-loop. SBP2 recruits the specific Sec-tRNA and the eFFsec elongation factor, which is necessary to insert selenocysteine into ribosomes.

During the catalytic cycle, ROOH peroxide is reduced to ROH; at this stage, the selenolated anion GPx-Se is oxidised by peroxide to a derivative of selenic acid GPx-SeOH. It uses GSH as a reducing substrate, as in the presence of this tripeptide, a link between selenium and cysteine sulphur is formed, which is then broken by a second molecule of GSH, producing GSSG (Figure 1.11).

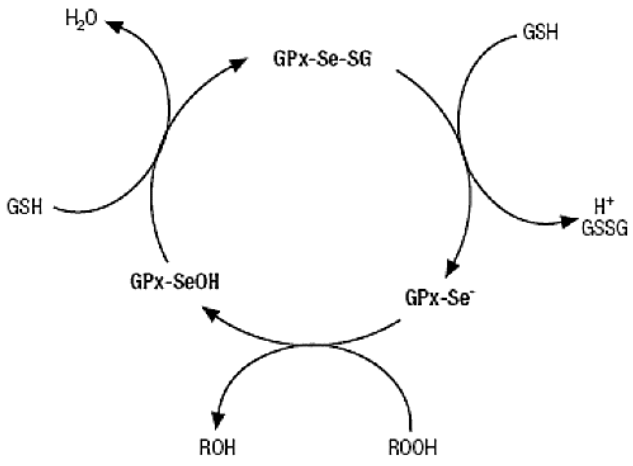

Figure 1.11. Reaction mechanism of Se-dependent GPx.

1.5.2.2.1. GPxs ISOFORMS

In mammals, the GPx family mainly comprise eight isoforms. However, many other GPxs have been identified in other organisms, almost all of which are not selenium-dependent.

- **GPx-1**

It is a selenium-dependent GPx, homotetrameric, with cytoplasmic localisation.

- **GPx-2**

Selenium-dependent, tetrameric, is expressed preferentially in the cytoplasm of enterocytes, although it has also recently been identified in the lungs. It is essential as a scavenger of hydroperoxides or lipid peroxides arising from the diet or metabolism of ingested xenobiotic substances.

- **GPx-3**

Homotetrameric is a selenium-dependent GPx expressed in various tissues in contact with body fluids, such as kidneys, placentas, lungs, gastrointestinal cells, thyroids, and hearts. As a reducing substrate, it can use GSH, but especially thioredoxin.

- **GPx-4**

It is a Se-dependent monomeric protein, acting specifically on lipid peroxides and phospholipid hydroperoxides. For this reason, it is also called phospholipid hydroperoxide GPx-PHGPx. It uses a large number of reducing substrates. It is the only GPx present at the mitochondrial level. It is involved in numerous physiological processes, such as sperm maturation and regulation of apoptosis.

- **GPx-5**

Non-Se-dependent, homotetrameric, it is secreted in the lumen of the epididymis of mammals, where it maintains the integrity of DNA in the sperms. It has a low efficiency (less than 0.1% compared to GPx-1.

- **GPx-6**

It is a Se-dependent isoform in some species, including humans, but not in mice. It is expressed exclusively in mammals at the embryonic level and in the olfactory system.

- **GPx-7**

It is a monomeric protein, not selenium dependent, expressed in various tissues. Although it has a reduced efficiency, its defect is related to breast carcinogenesis.

- **GPx-8**

  Non-Se-dependent monomeric protein was recently found in mammals and amphibians.

1.5.2.3. CATALASE (CAT)

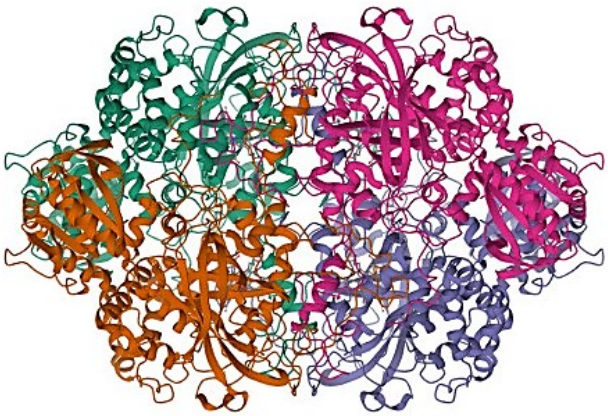

Figure 1.12. Crystal structure of catalase.

In 1900, Loew stated: "It seems that there is no plant and animal that lacks that peculiar enzyme, which the writer proposes to call "catalase" for its catalytic action on hydrogen peroxide" (Kirkman and Gaetani, 2007). In 1937, Sumner and Dounce obtained the crystallisation of bovine liver CAT (Zámocký and Koller, 1999). CAT (Figure 1.12) is a particularly large hemoprotein (240 kDa) composed of four identical subunits, each containing a heme group with Fe^{3+} at the active site. The conformation of the central nucleus of the CAT, about 300 residues, is remarkably conserved. In fact, it remains very similar to the CAT structure from phylogenetically distant organisms (Maté et al., 1999). There are three families of genes, virtually unrelated, that code for CATs capable of reducing H_2O_2: a manganese CAT, reported only in prokaryotes; a peroxidase CAT, widely distributed in the prokaryotic kingdom and also in lower eukaryotes; and the so-called true CATs, corresponding to homotetrameric heme-enzymes, ubiquitously present in eukaryotes but also many prokaryotes (Maté et al., 1999). CAT is located within subcellular compartments, in particular peroxisomes, and catalyses the reduction of H_2O_2 to water:

$$\mathbf{2H_2O_2 \rightarrow O_2 + 2H_2O}$$

The reaction takes place in two steps. In the first reaction, a molecule of H_2O_2 is reduced to water, leaving the enzyme as an oxoferryl intermediate called compound I (Maté et al., 1999). The enzyme is restored to a reduced state in the second step by reacting with another H_2O_2 molecule. CAT plays a crucial role in the adaptive response to H_2O_2 (Izawa et al., 1996),

suggesting an auxiliary role to GPx. Mutation studies have confirmed that acathalamic mice show increased susceptibility to oxidative damage (Srivastava and Ansari, 1980).

1.5.2.4. PEROXIREDOXINS (Prdx)

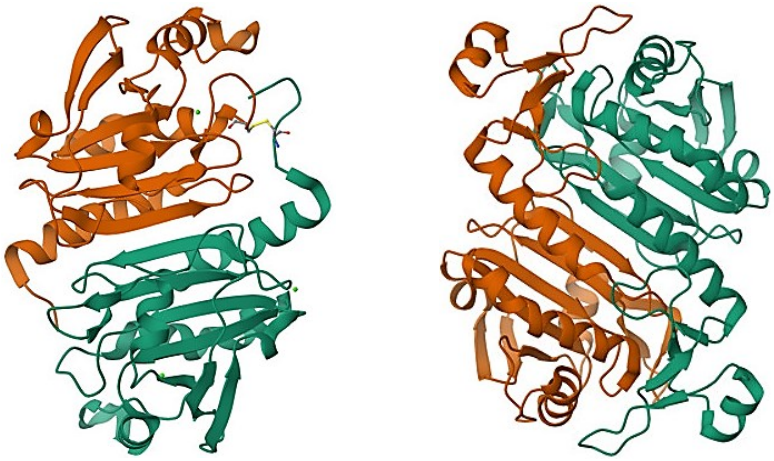

Figure 1.13. Crystal structure of peroxiredoxin1 (left) and peroxiredoxin6 (right).

Prdxs (Figure 1.13) are a multigene family of peroxidase-active enzymes ubiquitously in living organisms. The first peroxiredoxin was initially identified in yeast in 1987 and was called a thiol-specific antioxidant because it was thought to remove reactive sulphur species rather than ROS (Rhee, 2016). Today, it is known that Prdxs catalyse the reduction of organic and inorganic peroxides and their hydroxyl derivatives to water.

$$\mathbf{2Cys\text{-}SH + ROOH \rightarrow Cys\text{-}S\text{-}S\text{-}Cys + H_2O + ROH}$$

There are six Prdx isoforms, classified into three classes according to structure and mechanism of action:

- Typical two-cysteine Prdxs (Prdx1, Prdx2, Prdx3, Prdx4);
- Atypical two-cysteine Prdxs (Prdx5);
- One-cysteine Prdxs (Prdx-6).

The peroxiredoxin reaction consists of two steps (Figure 1.14) that rotate around a redox-active cysteine called cysteine peroxidase. The three classes share the first step: cysteine peroxidase attacks the peroxide substrate and is oxidised to S-hydroxycysteine Cys-SOH. The second step, which consists of cysteine regeneration, occurs differently in the three different classes.

- Typical 2-Cys Prdxs are homodimeric enzymes and contain two cysteine residues stored per subunit. Cys-SOH reacts with the Cys-SH of the other subunit to form an inter-subunit disulphide bridge.

- In atypical 2-Cys Prdxs, although homodimeric proteins, Cys-SOH reacts with Cys-SH belonging to the same subunit to form an intra-subunit disulphide bridge.
- In 1-Cys Prdxs, given the absence of a second cysteine, Cys-SOH is reduced by other proteins or small thiol molecules.

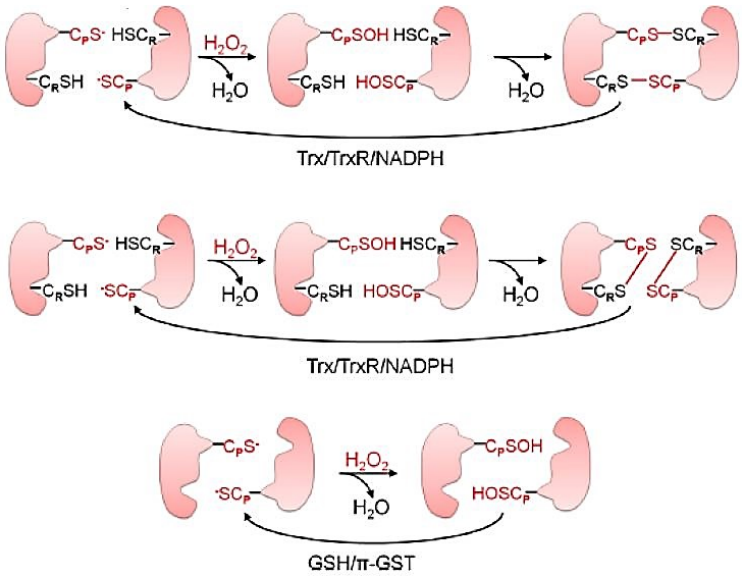

Figure 1.14. Reaction mechanism of typical 2-Cys, atypical 2-Cys and 1-Cys peroxiredoxins.

Oxidised Prdxs are then restored to a reduced state, thanks to the intervention of reducing agents, such as GSH, NADPH and thioredoxins (Trx).

1.5.2.4.1. Prdx ISOFORMS

- **Prdx1**

Prdx1 is a ubiquitously expressed nuclear and cytosolic 2-cysteine peroxidase protein. It is involved in multiple physiological processes, such as tumour suppression, inflammation, apoptosis, arteriosclerosis, and molecular chaperoning (Lee, 2020).

- **Prdx2**

Prdx2 is expressed in the cytosol and has a similar structure to Prdx1. Mouse Prdx1 and Prdx2 proteins share 89% sequence similarity and 74% sequence identity (Lee et al., 2020).

- **Prdx3**

Prdx3 is mainly located in the mitochondria. It is essential for the function of these organelles as a reduction in the activity of peroxiredoxin 3 reduces the production of ATP (Zhang et al., 2016).

- **Prdx4**

Prdx4 is mainly present at the endoplasmic reticulum level and secreted in the extracellular environment. In male mice, the knockout of the *prdx4* gene did not cause infertility but increased the risk of testicular atrophy; spermatogenic cells in *prdx4*$^{-}$ individuals are particularly prone to cell death due to oxidative stress (Lee, 2020).

- **Prdx5**

Prdx5 is the only isoform belonging to the family of atypical 2-Cys Prdxs in mammals; it is present in cytosol, peroxisomes and mitochondria. Prdx5 is implicated in various cellular processes, including the regulation of apoptosis and other cellular signalling pathways (Lee, 2020).

- **Prdx6**

Prdx6 is the only 1-cysteine isoform, and it is expressed at cytoplasmic and extracellular levels. Its extracellular localisation suggests a role in protecting cells from oxidative damage originating outside the cell. Prdx6 has phospholipase activity; this activity is involved in the repair and remodelling of the cell membrane and contributes to the detoxification of oxidised phospholipids. It protects the lungs from oxidative stress and helps prevent lung damage. A comparison of mice knockout for *gpx1* and *prdx6* (both are GSH-dependent peroxidases) reveals that Prdx6 is the main enzyme for reducing phospholipid hydroperoxides in the lung (Lee, 2020). Two different variants of Prdx are known in fish: Prdx6a and Prdx6b; they can play an alternative role in the antioxidant response in fish exposed to heat stress (Tolomeo et al., 2016).

2. AIM OF THESIS

The scientific community's focus in recent years has been on so-called "emerging contaminants", among which are the per- and polyfluoroalkyl substances (PFAS). What has raised the most significant concern is the high persistence of these chemicals in the environment and their high potential for bioaccumulation within organisms. For this reason, the focus has shifted from acute exposure studies to investigating the possible effects of chronic exposure to these substances. In particular, a pulse in studying these compounds came from detecting PFAS in human blood. The Veneto region is one of the most emblematic cases of PFAS contamination. In addition to being a risk to human health, PFAS represent a potential risk to the health of organisms, particularly aquatic ones. How PFAS act within organisms remains unknown. One hypothesis is that they can act directly on cellular substrates, causing damage, such as inactivation of proteins or alterations of membrane lipids. Furthermore, their role as endocrine disrupters is well-known. Otherwise, PFAS can also alter the cellular redox balance, forming reactive oxygen species (ROS) and resulting in oxidative stress with consequent damage to cellular structures. For this reason, organisms have developed a series of antioxidant defences. Xenobiotic substances such as PFAS can determine an alteration in the physiology of organisms, which can be evaluated by using a multi-biomarker approach to test the stress response at the level of the antioxidant system.

This study aims to understand how chronic exposure to PFAS can induce physiological responses of aquatic organisms in relation to different environmental concentrations of these pollutants. For this study, the *Squalius cephalus* species, commonly known as chub, ubiquitary living in the rivers of the Veneto region, has been used. The organisms were sampled in three different rivers with three different concentrations of PFAS: Leogra Torrent, defined as a "very low polluted" site; Roggia Moneghina, described as a "low polluted" site; Retrone River, designated as a "highly polluted" site. The sampling activity took place on 19 March 2021.

A previous study analysed the liver of these specimens, highlighting a possible species-specific response to PFAS exposure due to the *S. cephalus* lifestyle with respect to that of a benthic species (*Padogobius bonelli*) (Piva et al., 2022). Here we wanted to investigate further the physiological responses resulting from chronic exposure to PFAS in the kidney of *S. cephalus*. In fact, the kidney represents a potential site of PFAS accumulation and the responsible organ for their elimination. This physiological role could contribute to the increase of ROS production in the organ, with a consequent rise in oxidative stress risk.

The available biological samples were analysed using molecular biology and biochemical methods to verify this hypothesis. Regarding the molecular biology analysis, the expression of genes encoding for four antioxidant enzymes, SOD, GPx, CAT, and Prdx, was measured at the transcriptional level. Their up- or down-regulation was evaluated in relation to the different environmental conditions. In particular, various isoforms of these enzymes were considered (*sod1*, *sod2*, *gpx1*, *gpx4*, *cat*, *prdx1*, *prdx2*, *prdx3*, *prdx4*, *prdx5*, *prdx6a*) to evaluate the protection role of alternative isoforms of the same enzyme in different cellular compartments. For example, differential gene expression of cytoplasmic SOD1 and GPx1 compared to mitochondrial SOD2 and GPx4. The expression of various Prdx isoforms was evaluated and correlated to their different cellular compartmentalisation. Regarding biochemical analyses, some enzymatic assays were performed to assess the levels of active proteins of SOD, GPx and CAT. Finally, two biochemical tests were applied to verify the oxidative cellular damage to lipids and proteins.

3. MATERIALS AND METHODS

3.1. TARGET SPECIES: *Squalius cephalus*

In the present study, the species *Squalius cephalus* (Linnaeus 1758), previously classified as *Leuciscus cephalus* and commonly known as European chub (Figure 3.1), was analyzed. It belongs to the Leuciscidae family, commonly called Cypriniformes (Table 3.1), a group widely distributed in the freshwaters of Central Europe, partly due to anthropogenic introduction.

SCIENTIFIC CLASSIFICATION	
Domain	Eukaryota
Kingdom	Animalia
Phylum	Chordata
Class	Actinopterygii
Order	Cypriniformes
Family	Cyprinidae
Subfamily	Leuciscinae
Genus	*Squalius*
Species	*S. cephalus*

Table 3.1. Taxonomy of Squalius cephalus

Naturally absent in Italy, it has only been imported for a few decades; here, although massive introductions by humans have made it complicated to trace its original distribution, it is considered native to Northern and Central Italy (Balestrieri, 2006). In Italy Cypriniformes include 34 species, of which the chub is one of the most common and widespread taxa of the entire peninsula.

Figure 3.1. Specimen belonging to the Squalius cephalus species.

With an average size of 15-20 cm, it presents a wide variability in dimensions, with individuals capable of reaching up to 60 cm in length. Chub is characterized by an elongated body, laterally compressed and covered with ctenoid scales. The head, relatively large in proportion to the body, has a terminally positioned mouth and well-developed eyes. It has a dark-colored homocercal tail, like the dorsal fin; the pectoral fins instead have a lighter, almost transparent color; the pelvic fins and the anal fin are

red. The body has the usual counter-color with a darker back, tending towards grey-blue, while the belly appears light and silvery in color. The tapered and hydrodynamic shape gives it efficient swimming performance; in fact, it has a typically mobile lifestyle in the water column. Although it prefers warm waters, it possesses extensive ecological plasticity (Balestrieri et al., 2006). The chub is indeed abundant in small rivers and large streams, but it is also found in slow-flowing lowland rivers and very small mountain streams (Kottelat and Freyhof, 2007).

Despite its ubiquity and large number in terms of individuals, the chub has never been long used to study anthropogenic pollution (Freyhof, 2014). However, given its wide diffusion, as well as being a generalist species (able to live even in the most polluted waters), in recent years its use has increased to evaluate the levels of contamination of water bodies and provide relevant information on the state of danger (vulnerability) of aquatic organisms (Nyeste et al., 2019), proving to be a good bioindicator for pollution.

3.2. SAMPLING SITES

For sampling, three waterways characterized by different levels of PFAS contamination were selected, all located in the province of Vicenza and belonging to the Leogra-Bacchiglione basin (Figure 3.2).

Figure 3.2. Map of Veneto Region with focus on the three sampling sites.

Data recording PFAS pollution in the three target rivers are provided by ARPAV (Regional Agency for Environmental Prevention and Protection of Veneto), which has been monitoring PFAS pollution in over 200 river and lake sites on a constant frequency since 2013. The substances analyzed by the Regional Laboratories Department of the ARPAV are the following: PFOA, PFOS, PFBA, PFBS, PFPeA, PFHxA, PFHpA, PFHxS, PFNA, PDFeA, PFUnA, PFDoA, PFHpS. Since 2018, HFPO-DA and C6O4 have also been detected.

Leogra Torrent, in Torrebelvicino (VI) (45.71779193 N; 11.30627616 E), was chosen as the "very low polluted" site, which acts as a control. With variable flow depending on the season and the frequency of rainfall, it benefits from the contribution of numerous tributaries and it is characterized by a typical torrential regime. Being located upstream of the pollution source, the concentration of PFAS was, at the time of sampling, lower than the detection threshold (< 5 ng/L).

Roggia Moneghina River, located in Grumolo delle Abbadesse (VI) (45.5116 N; 11.6560 E) has been identified as a "low polluted" site. It is an artificial canal of modest capacity used mainly for irrigation. On the sampling date, the PFAS concentration was 5.64 ng/L.

Retrone River, in Altavilla Vicentina, was chosen as the "highly polluted" site. It flows near the city of Vicenza and is an important tributary of the Bacchiglione. It is a waterway with a high level of pollution, probably due to various kinds of industrial wastes and, passing through the city, also due to urban wastes. Being located downstream from the source of pollution, it is the site where the highest concentration of PFAS was found. The last ARPAV detection prior to sampling recorded a total PFAS content of 582,6 ng/L.

For uniformity of name, during the thesis, Torrente Leogra will be identified as "Site 1" or "Very low polluted site", Roggia Moneghina as "Site 2" or “Low polluted site" and Retrone as "Site 3" or "Highly polluted site" (Table 3.2).

SITE	Date of last detection	PFAS (ng/L)
1. Torrente Leogra	01/10/2019	< 5
2. Roggia Moneghina	02/09/2019	5.64
3. Retrone	27/06/2018	582.6

Table 3.2. PFAS concentration in the sampling sites (monitoring data provided by ARPAV before sampling activity).

In choosing the target sites, some conditions were considered, namely the similarity of the waterways from both points of view of the flow rate and chemical-physical parameters (temperature and oxygenation).

3.3. SAMPLING ACTIVITY

The sampling activity was carried out on 19 March 2021 in a single day to avoid inserting variables, due for example to weather and temperature, which could in turn modify the chemical-physical parameters of the water.

Fifteen samples were taken for each site, of comparable size to each other in order to avoid influencing factors related to age and size. To minimize the stress induced by sampling, the electrofishing technique was used, using a high-voltage instrument. A generator produced alternating current, converted into direct current at different voltages by an alternator and transmitted to two electrodes (anode and cathode). The correct voltage was chosen to obtain the best result based on several factors, both physical and biotic. Among the physical parameters, the morphology of the river (average width and depth), the type of seabed and the conductivity of the water were considered. Among the biotic factors, the size of the species under examination was considered in particular. Once captured, the specimens were immediately sacrificed using an overdose of anesthetic, using Clove Oil at a concentration of 0,0070 ml/L, obtained from *Syzygium aromaticum* . It is a natural substance, low cost and low toxicity. The fish were placed in plastic bags and transported to the laboratory, in refrigerated containers.

3.4. SAMPLE PREPARATION

The organisms were immediately dissected, on the same day as sampling; the organs of interest (intestine, gills, muscle, liver, kidney and gonads) were removed and inserted into tubes marked with an alphanumeric code. The reference species, sampling site, study organ and individual number were indicated. The samples were stored at -80°C.

3.5. MOLECULAR ANALYSES

3.5.1. RNA EXTRACTION

Kidney samples were processed by the guanidine thiocyanate-phenol-chloroform method to extract total RNA content. RNA is a particularly sensitive and easily degradable structure, due to RNases, enzymes that catalyze the hydrolysis of the macromolecule; therefore, the extraction procedure requires great care and all reagents must be treated with RNase inhibitors. 10 individuals per site were used, for a total of 30 samples. For each sample, approximately 100 mg of tissue were used and then

transferred to a 1.5 ml Eppendorf tube. To homogenize the tissue, 1 mL of TripleXtractor™ (Grisp) was added; it is an acidic chemical compound, composed of guanidine thiocyanate, which promotes cell lysis and phenol, which denatures proteins. Guanidine thiocyanate also preserves the integrity of RNA by denaturing RNases. Tissues were mechanically homogenized with a pestle. 200 µL of chloroform was added, which completes the denaturation of the proteins, removes the lipids, thanks to its high density, and facilitates the separation of the phenolic phase from the aqueous one (containing the nucleic acids). The acidic pH of TRIzol favors the precipitation of DNA in the phenolic phase. The subsequent centrifugation for 30 minutes at 13000 rcf allowed the separation of the phases (Figure 3.3): in the lower part of the Eppendorf remains the heavier organic phase with the largest macromolecules (lipids, carbohydrates, proteins and mainly phenols); the interphase contains the DNA; the aqueous phase contains the RNA.

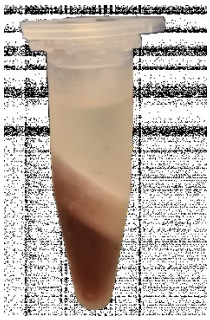

Figure 3.3. Phase separation: organic phase, interphase and aqueous phase.

For each sample, the aqueous phase was transferred to another Eppendorf; to precipitate the RNA in solution, 500 µL of isopropanol were added and the samples were centrifuged for 15 minutes at 13000 rcf. The deposited pellet (Figure 3.4) was washed twice with 1 mL of 75% ethanol to remove precipitated salts and centrifuged at 7500 rcf for 5 minutes.

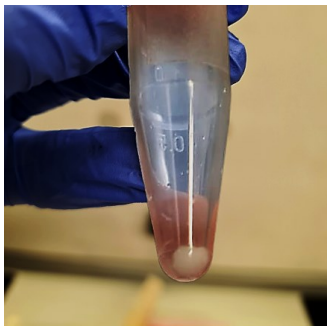

Figure 3.4. Pellet formation due to the RNA precipitation with isopropanol.

Once the supernatant was removed, the pellet was completely dried under a laminar flow hood for 10 minutes. The pellet was then resuspended in a volume of RNase-free H_2O proportional to the quantity of pellet for

approximately 2 hours. The samples were incubated in a thermal bath at 55°C for 10 minutes and then analyzed.

3.5.1.1. RNA QUANTIFICATION

To quantify the RNA present in the samples, the NanoDrop™ ND-1000 (Thermo Scientific) (Figure 3.5) was used, a spectrophotometer capable of measuring absorbance in small volumes of solution (1 µL of total RNA). The instrument works in an RNA concentration range between 2 and 3000 ng/µL.

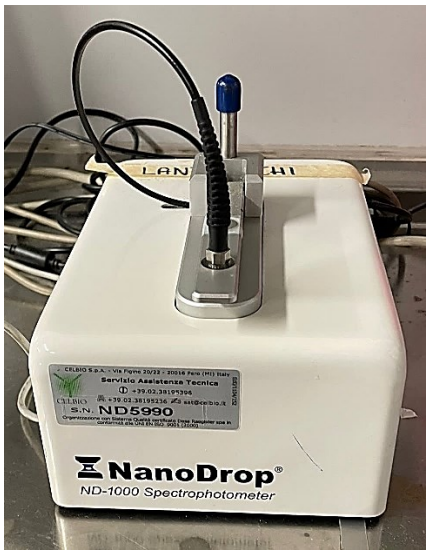

Figure 3.5. The NanoDrop™ ND-1000 (Thermo Scientific) spectrophotometer.

The quantity of RNA was obtained by measuring the absorbance at 260 nm, the wavelength at which the absorbance peak of the nucleic acids, DNA and RNA is recorded, due to the presence of the aromatic rings of the nitrogenous bases. An example of the absorbance spectrum of RNA is represented in Figure 3.6. The RNA concentration was obtained by multiplying the absorbance by an RNA-specific constant (40 ng/µL). The purity of the RNA samples was also assessed at NanoDrop. To exclude contamination by proteins and DNA, the absorbance was measured at 280 nm (wavelength at which the absorbance peak of the proteins caused by the presence of amino acids with aromatic rings is recorded) and the ratio 260/280 was calculated. RNA samples having a 260/280 ratio between 1,9 and 2,1 were considered pure (if lower it would have meant protein contamination; if higher, DNA contamination). To exclude contamination by phenols and lipids, the absorbance was measured at 230 nm (wavelength at which the peak of other compounds such as carbohydrates and phenols that could have remained in solution occurs) and the 260/230 ratio was calculated. Samples having a 260/230 ratio greater than 2,2 were considered pure.

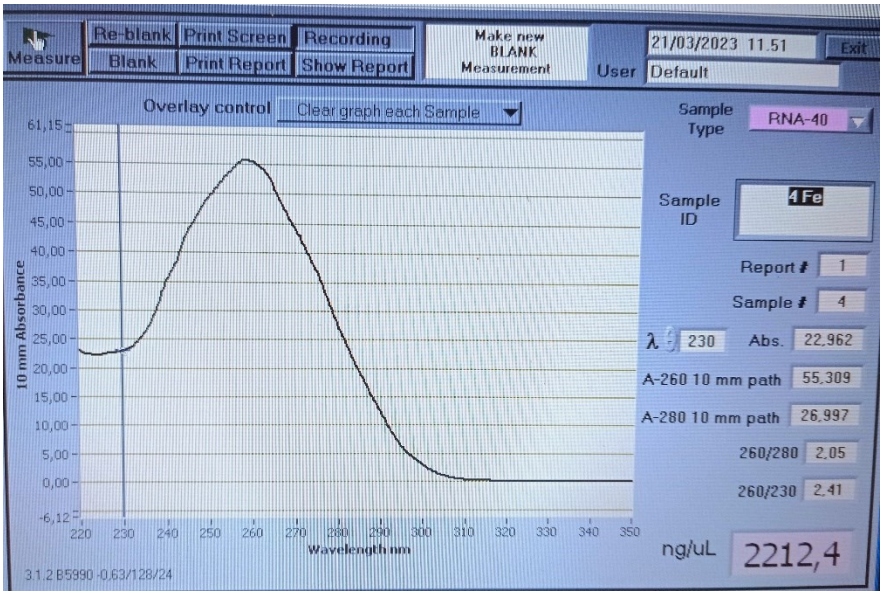

Figure 3.6. Example of the absorbance spectrum of a pure RNA sample.

3.5.1.2. ASSESSMENT OF RNA INTEGRITY

To evaluate the integrity of the RNA, 1% agarose denaturing gel electrophoresis was carried out on a 5 µL aliquot for each sample, to which 1 µL of loading dye was added. The mRNA represents only 1-3% of the total RNA, it is therefore not visible on gel, while rRNA represents more than 80% of the sample and for this reason can be visualized on gel. Electrophoresis clearly showed the two bands corresponding to 18S rRNA and 28S rRNA, indicating good integrity of the samples (as in Figure 3.7). Streaked bands or a 28S:18S band intensity ratio less than 2:1 would have indicated poor RNA quality.

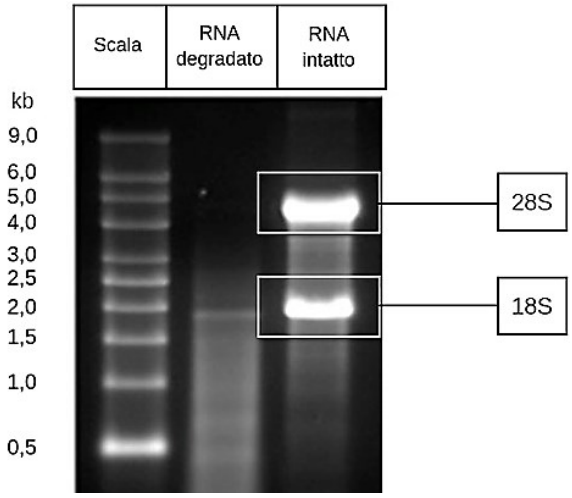

Figure 3.7. Example of a gel electrophoresis on a degraded RNA sample compared to a good quality RNA sample.

3.5.2. REVERSE TRANSCRIPTION AND cDNA SYNTHESIS

For the subsequent evaluation of gene expression, RNA samples were reverse transcribed to cDNA using the cDNA Synthesis Kit (biotechrabbit). The samples were previously diluted to normalize the concentration to a value of 50 ng/µL. The Mix prepared for each microliter of sample included:

- 1 µL of RevertUP™ II Reverse Transcriptase capable of promoting cDNA synthesis (>19 kb) with good efficiency even at low template concentrations, with greater thermostability;
- 0.5 µL of RNase Inhibitor, an RNase inhibitor to preserve the integrity of the RNA;
- 2 µL of dNTP Mix;
- 4 µL of 5x Reverse Transcriptase Buffer;
- 11 µL of PCR Grade Water;
- 0,5 µL of Oligo (dT), a primer capable of pairing with the polyA tails of the mRNA in order to discriminate the mRNA from other RNAs present in the sample.

PCR tubes containing 19 µL of Mix and 1 µL of sample were incubated inside a thermocycler at 50 °C for 60 minutes (Figure 3.8) to ensure primer pairing and subsequent chain elongation and subsequently at 99 °C for 5 minutes to inactivate the enzymes. The cDNA samples, concentrated 50 ng/µL were stored at -20 °C.

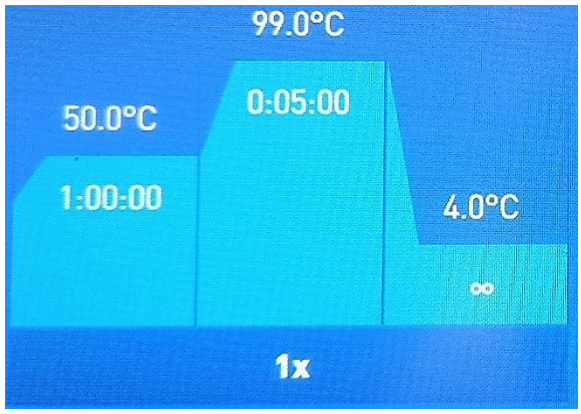

Figure 3.8. Thermocycler display showing time and temperature for each step of reverse transcription.

3.5.3. PRIMER DESIGN

To evaluate gene expression, specific primers were designed for each individual gene of interest. Only for the *sod2* and *gpx4* genes the *Squalius cephalus* gene sequences were known, on which it was, therefore, possible to build primers. For the other genes of interest (*gpx1*, *cat*, *sod1*, *prdx1*, *prdx2*, *prdx3*, *prdx4*, *prdx5*, *prdx6a*), however, as there are no known gene sequences

relating to the *Squalius cephalus* species, primers were designed on gene sequences belonging to phylogenetically related species, present in the NCBI GenBank® database. Therefore, a comparison was previously carried out between the species under examination and other teleost species to deduce the most similar ones, using the NCBI BLAST® tool. From this analysis, the greatest similarity emerged with the species *Pimephales promelas*, (also belonging to it to the Cypriniformes family), therefore used for the construction of *gpx1, cat, prdx1, prdx2, prdx3, prdx4, prdx5, prdx6a* primers. Regarding *sod1*, it was decided to build the primers on another species of Leuiscidae, namely *Carassius auratus*. Primers for the *gapdh* gene were also designed on *Pimephales promelas*, used in this study as a housekeeping gene, expressed at a basal level as it is essential for correct cellular functioning and therefore theoretically not influenced by exposure to PFAS.

Primer3 v 4.1.0 program (primer3.ut.ee/) was used to construct primers. The parameters were optimized to ensure the maximum reliability of primers in subsequent gene expression analyses. In particular:

- Length: 18 - 24 bp (optimum 20 bp);
- Melting temperature: 62 °C – 67 °C (optimum 64 °C);
- Maximum difference between melting temperatures of the two primers: 2 °C;
- Percentage in GC: 55%.

Generated primer pairs were analyzed using the IDT OligoAnalyzer™ tool (eu.idtdna.com/calc/analyzer). Among the parameters, the following were considered:

- Probability of hairpin formation ($\Delta G < 3$);
- Probability of intra-chain pairings within the single primer (self-dimer: $\Delta G > -9$);
- Probability of pairings between primer fw and primer rv (hetero-dimer $\Delta G > -9$);
- Number of pairings at the 3' end, preferably not exceeding 3.

A subsequent analysis was performed with the Beacon Designer™ program (premierbiosoft.com/qOligo/Oligo.jsp?PID=1). It was rated:

- Cross-dimer ($\Delta G > -3.5$);
- GC clamp (maximum 2).

Only primer pairs that met these parameters were selected. Since they were not constructed directly on chub, to have the reasonable certainty that the primers can also work in the species under examination, it was verified that they fell within genetic regions conserved during evolution. A multiple

alignment was then performed with the GenomeNet ClustalW program (Multiple Sequence Alignment - CLUSTALW (genome.jp), using sequences belonging to the most phylogenetically related species. Only primers located in regions with a degree of conservation greater than 80% were retained.

3.5.4. ASSESSMENT OF PRIMER BY PCR

The chosen primers were experimentally tested to verify their correct functioning. A PCR was performed using chub cDNA as a template. For each primers pair the following reagents were used:

- 12,5 µL of YourTaq Mix;
- 6,5 µL of PCR Grade Water;
- 3 µL of cDNA;
- 1,5 µL of fw primer;
- 1,5 µL of rv primer.

PCR tubes were incubated in the thermocycler set with the following parameters (Figure 3.9):

- Initial activation: 2 minutes at 95 °C (this favors complete denaturation of the cDNA);
- Annealing (35 cycles): 30 s at 95 °C (denaturation), 30 s at the chosen annealing temperature (annealing), 30 s at 72 °C (extension).
- Extension: 5 minutes at 72°C to ensure the amplicons have been fully amplified.

Figure 3.9. Thermocycler display showing time, temperature and number of cycles for each PCR step.

Primers were tested with different annealing temperatures (57 °C – 60 °C – 63 °C). Too high annealing temperatures would have resulted in a low reaction efficiency with a limited number of pairings and, therefore, a reduced amplicon concentration. Conversely, a too low annealing temperature would have meant a high efficiency of the reaction with a greater number of pairings but also an increased risk of non-specific pairings (less specificity).

Gel electrophoresis was then performed to visualize the PCR products (as in Figure 3.10). Given the small size of the amplicons, a 2% agarose gel was used; 2,4 g of agar were dissolved in 120 ml of 1x TAE buffer, to which 12 µL of FluoroVue™ Nucleic Acid Gel Stain (SMOBIO) was added. A 50 bp DNA ladder (biotechrabbit) was used proportionally to the gel concentration. For each amplicon, a 5 µL aliquot was loaded into the gel, to which 1 µL of DNA Loading Dye (biotechrabbit) was added. Only primers that gave a positive result were used in subsequent gene expression analyses by real-time PCR.

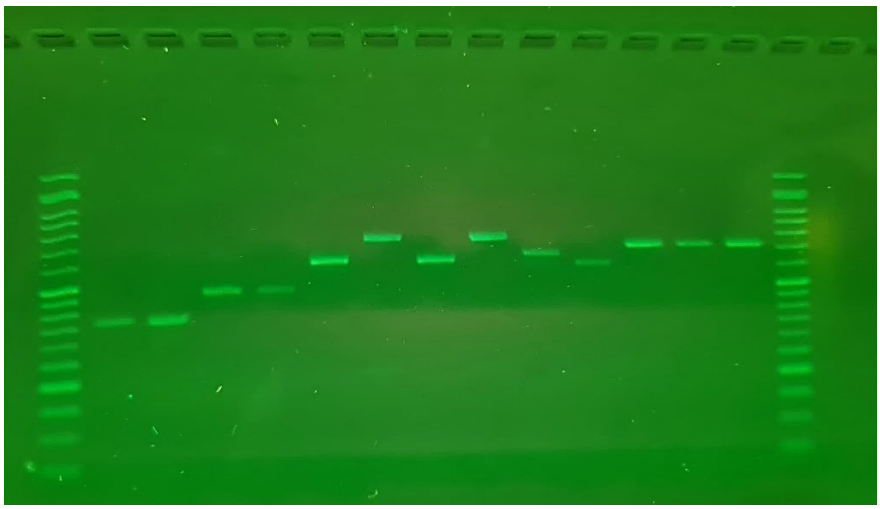

Figure 3.10. Results displayed under UV light of an electrophoresis gel for primer testing.

3.5.5. QUANTIFICATION OF GENE EXPRESSION BY qRT-PCR

For gene expression analyses, qRT-PCR was performed. A calibration line was then constructed for each gene, to be able to compare the Ct of the samples with the Ct of the standards of known quantity. The Ct represents the cycle at which the concentration of the amplified reaches the threshold line, set manually by the operator, positioned approximately halfway through the exponential phase (in this phase at each cycle the number of DNA molecules doubles). To construct the calibration line, a pool of cDNA from different individuals was used, per site, in order to evaluate the efficiency of the primers on all individuals and to avoid individual-specific responses. The cDNA pool was used at scalar concentrations: 100 ng/µL, 50 ng/µL, 25 ng/µL, 12,5 ng/µL. The analyses were carried out in 3 replicates, as illustrated in the following Table 3.3.

Primer	**cDNA concentrations (ng/µL)**											
1	100	100	100	50	50	50	25	25	25	12,5	12,5	12,5
2	100	100	100	50	50	50	25	25	25	12,5	12,5	12,5
3	100	100	100	50	50	50	25	25	25	12,5	12,5	12,5
4	100	100	100	50	50	50	25	25	25	12,5	12,5	12,5

Table 3.3. Example of dilution scheme on the RT plate to construct the standard curve.

The chemical dye SybrGreen was used, a fluorescent molecule capable of intercalating nonspecifically into the minor groove of double-stranded DNA. Fluorescence emission occurs only during the extension phase of the PCR; at each cycle, there is an increase in fluorescence due to the increasing number of DNA copies. The qPCRBIO SyGreenMix (PCR BIOSYSTEMS) was used, containing, in addition to the dye, also dNTPs, Taq polymerase and $MgCl_2$. The passive reference dye ROX was used to normalize the change in fluorescence not related to the PCR reaction. The following quantities were used for each well:

- 5 µL of qPCRBIO SyGreenMix;
- 2 µL of PCR Grade Water;
- 1 µL of forward primer;
- 1 µL of reverse primer;
- 1 µL of DNA.

The following parameters were set for qRT-PCR (Figure 3.11):

- Initial denaturation: 2 min at 95°C;
- 40 annealing and extension cycles: 20 s at 95°C and 60 s at 60°C;
- Dissociation: 15 s at 95°C, 1 min at 60°C, 15 s at 95°C, 15 s at 60°C.

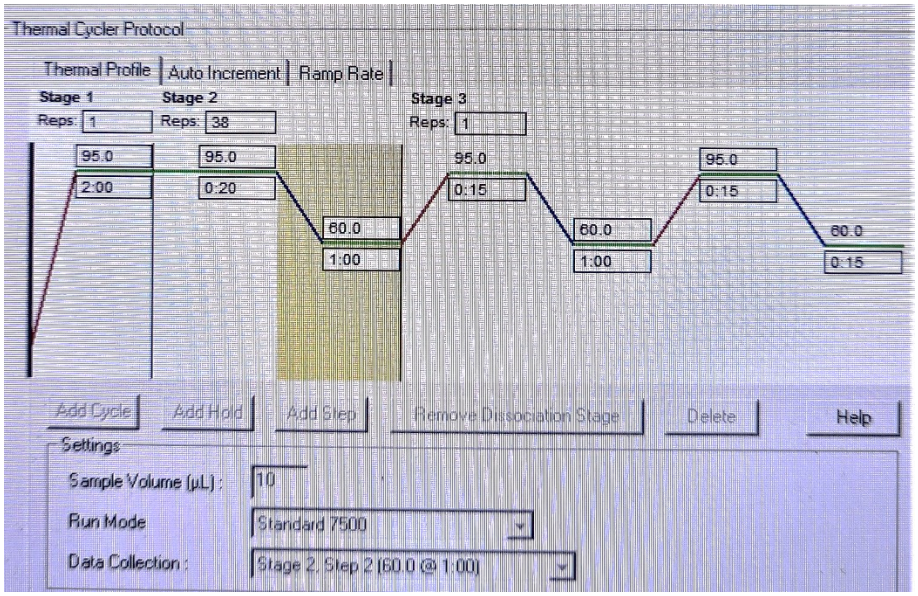

Figure 3.11. Applied Biosystems® 7500 Fast Real-Time PCR System display showing time, temperature and number of cycles for each qRT-PCR step.

The optimal efficiency (100%) is represented by a slope of the calibration line equal to -3.5. An attempt was made to optimize the analyses using primers with similar efficiencies, comparable to each other and close to maximum. The specificity was verified again by visualizing the dissociation curve. The presence of a single peak indicated correct primer specificity; on the other hand, the visualization of two or more peaks indicated the

amplification of a non-specific fragment or the formation of primer dimers (Figure 3.12).

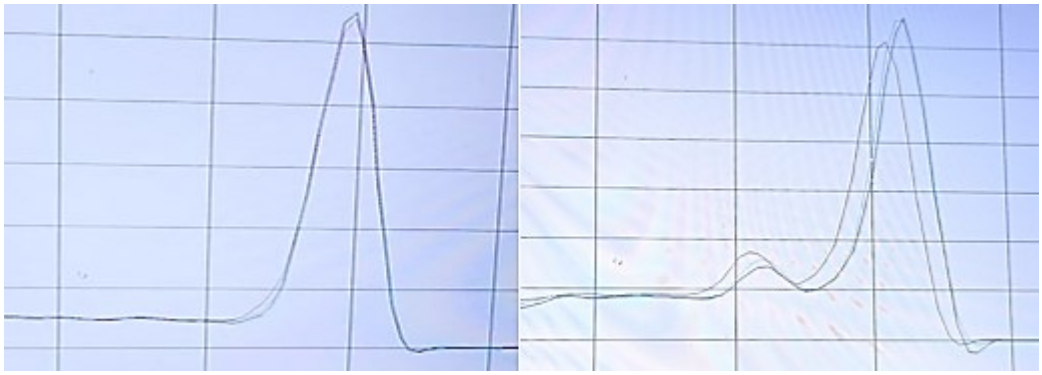

Figure 3.12. Example of the dissociation curve of a specific amplicon (left) and a nonspecific amplicon with probably primer dimers (right).

Primers showing the best efficiency and specificity were used in subsequent qRT-PCRs for each sample (Table 3.4). For gene expression analyses, eight samples per site were randomly selected. Gene expression levels were normalized to the expression levels of the housekeeping gene *gapdh*. The analyses were carried out in three replicates.

GENE	PRIMER	SEQUENCES 5′ -> 3′	amplicon (bp)	T annealing
sod1	5_SOD1_C.auratus_F	GGTCCGCACTACAACCCTCA	200	57°C
	5_SOD1_C.auratus_R	CCCAAGTCATCCTCTTTCTCGTGG		
sod2	5_SOD2_S.cephalus_F	AGTCTCCCTTCAGCCTGCATTG	170	63°C
	5_SOD2_S.cephalus_R	CAGCGGACATCATCTCCTTCATCT		
gpx1	2_GPX1b_P.promelas_F	TCCATTCCCATTCGATGACCCAAT	126	60°C
	2_GPX1b_P.promelas_R	GGCACTCCATCAGAACCGATAAGA		
gpx4	2_GPX4_S.cephalus_F	CGGGACAGAAGCGGACATCAA	145	63°C
	2_GPX4_S.cephalus_R	TCCCAGAGTTCCCTTGCCTTTG		
cat	1_CAT_P.promelas_F	GCGTCCTGAATCGTTGCACCA	120	60°C
	1_CAT_P.promelas_R	TGACCCTCAGCGTTGACCAGT		
prdx1	2_PRDX1_P.promelas_F	AAGGTCCCTCTGGTGGCAGATT	148	60°C
	2_PRDX1_P.promelas_R	CCACTGGCAGGTCATTGATGGT		
prdx2	1_PRDX2_P.promelas_F	TCCACCGACTCTCACTTCAG	125	60°C
	1_PRDX2_P.promelas_R	ACGCCGTAATCCTGGGAGATG		
prdx3	1_PRDX3_P.promelas_F	GGCACTGCTGTTGTCAATGGA	127	60°C
	1_PRDX3_P.promelas_R	TGAAGGCGATGATCTCTGTGG		
prdx4	3_PRDX4_P.promelas_F	GTTCGGTGGACTCGCAGTTTACTC	158	60°C
	3_PRDX4_P.promelas_R	TCTGAGTGTGTGTCCCTGATCCTC		
prdx5	2_PRDX5_P.promelas_F	CACTCCACACGCATTTCCAGCA	144	60°C
	2_PRDX5_P.promelas_R	TCCTGGCACAGCAAAAAGCACT		
prdx6a	3_PRDX6a_P.promelas_F	TCACTGCCCGTTGTGTGTTTGTG	172	60°C
	3_PRDX6a_P.promelas_R	TCTTGACCAGGCTTCCAGTCCAC		
gapdh	GAPDH_P.promelas_F	ATCACAGCCACACAGAAGAC	126	60°C
	GAPDH_P.promelas_R	AGGAATGACTTTGCCCACAG		

Table 3.4. List of primer pairs used for qRT-PCR, with amplicon size (bp) and annealing temperature (°C).

To calculate the gene expression the ΔΔCt method was used. The Ct for each sample was normalized, subtracting the Ct of the housekeeping gene *gapdh*,

to obtain a first ΔCt. For the very low polluted site (control site) an average of the ΔCt of the samples was made for each analysed gene. The ΔCt of each sample from all three sites were normalized, subtracting the highest mean, to obtain a second ΔΔCt. In this way all gene expression values were normalized on the same reference, making it possible to compare different enzymes and different sites.

Gene expression for each gene was calculated by the following formula:

$$gene\ expression = 2^{-\Delta\Delta Ct}$$

3.6. BIOCHEMICAL ANALYSES

To perform all biochemical analyses, tissue samples were homogenized using a homogenization buffer, an aqueous saline solution containing:

- Tris-HCl 20 mM, pH 7,6;
- EDTA 1 mM;
- DTT 1 mM;
- Sucrose 0,5 M;
- KCl 0,15 M.

Homogenization was performed through mechanical crushing of the tissue, using a high-speed mixer-homogenizer (Polytron PT 3000, Kinematica AG, Homogenizer Mixer) for the time necessary to obtain a homogeneous solution. Centrifugation at 13000 rcf followed, for 30 minutes at 4 °C; the supernatant was transferred to new Eppendorf and divided into different aliquots, then stored at -80°C.

3.6.1. TOTAL PROTEIN QUANTIFICATION

The protein content of the cell extract is determined using the phenolic reagent Folin-Ciocalteau (Lowry et al., 1951), which allows the determination of a protein quantity between 5 and 100 µg in 0,2 ml of sample. The protein concentration of each sample, expressed in mg/ml, is calculated by linear regression between known and increasing amounts of standards (BSA 1 mg/ml in homogenization buffer) and their absorbance values at 750 nm.

The following solutions were prepared:

- A solution: Na_2CO_3 2% NaOH 0,1 M. 4 g NaOH + 20 g Na_2CO_3 in 1 L of H_2O milliQ.
- B solution: $CuSO_4x5H_2O$ 0,5% in sodium citrate 1%. 1 g tri-sodium citrate + 0,5 g $CuSO_4x5H_2O$.
- C solution: 25 mL of A solution + 0,5 mL of B solution (ratio 1:50).
- D solution: 1,36 mL of H_2O + 1 mL FOLIN.

A standard curve was constructed using increasing doses of albumin in known quantities. In each glass tube, a volume of H_2O was added such that, when added to the volume of albumin, the total added volume was 200 µL, as in the following Table 3.5:

N° glass tubes	1	2	3	4	5	6	7	8	9	10	11	12
ALBUMIN (µL)	0	0	5	5	10	10	20	20	30	30	40	40
H_2O milliQ (µL)	200	200	195	195	190	190	180	180	170	170	160	160

Table 3.5. Dilution scheme for standard curve for Lowry assay.

At each tube 1 ml of solution C was added, and then vortexed. After 10 minutes of waiting, 100 µL of solution D were added and briefly vortexed. After 30 minutes, the absorbance at a wavelength of 750 nm was read.

For the reading of the samples, the volumes of albumin were replaced with 4 µL of cell extract, to which 196 µL of H_2O were added. For blanks, the sample was replaced with an identical volume of homogenization buffer. Both samples and blank were performed in duplicate. Similarly to the calibration line, 1 ml of solution C was added to each sample. 100 µL of solution D was added after 10 minutes. The absorbance at 750 nm was read after 30 minutes.

The standard curve has a linear equation y = bx + a, where y represents the absorbance and x represents the protein concentration to be determined (x=(y-a)/b). For each double, the average was calculated and normalized by subtracting the blank mean. Then, the result was divided by the sample volume (to obtain the result in µg/mL) and then multiplied by 0,001 to obtain a protein concentration in mg/mL:

$$\text{mg proteins/mL} = \frac{0{,}001\left(\frac{y-a}{b}\right)}{\text{sample Volume}}$$

3.6.2. SOD ACTIVITY ASSAY

To quantify superoxide dismutase activity, an enzymatic assay was performed. The reaction rate was deduced by measuring the change in absorbance during the enzyme kinetics. The assay is based on the activity of xanthine oxidase, which catalyzes the oxidation reaction of hypoxanthine to xanthine and then uric acid, causing the formation of free radicals, including superoxide ions. The latter, in the absence of SOD, act on cytochrome c^{3+}, reducing it to cytochrome c^{2+}; this determines a color variation and a consequent increase in absorbance. The SOD present in the sample, instead, dismutates the superoxide ions, preventing the reduction of cytochrome c^{3+}; in this case, however, a slight increase in absorbance is recorded, although much lower than the increase measured in the absence of this enzyme. Therefore, it is an indirect assay, based on the ability of the

SOD enzyme to eliminate $\bullet O_2^-$ and consequently to inhibit the reactions caused by this radical.

Enzyme activity is expressed as U/mg of protein, with one unit of SOD defined as the amount of enzyme that causes a 50% inhibition of the reduction reaction of oxidized cytochrome.

The following solutions were prepared:

- SOD buffer: 1,36 g of KH_2PO_4 in 200 mL of H_2O + 2,67 g of Na_2HPO_4 x $2H_2O$ in 300 mL of H_2O + 0,019g of EDTA + 0,033 g NaN_3 (pH 8,6);
- Hypoxanthine solution: 0,018 g in 8 mL of H_2O + 2 mL of NaOH (1 M);
- Cytochrome c solution (1,6 mM): 0,02 g in 1 mL of phosphate buffer;
- Xanthine oxidase solution: 100 µL of xanthine oxidase + 8 mL of H_2O.

Cuvettes were set up with the following composition, illustrated in Table 3.6:

		SAMPLE	BLANK
REAGENTS	SOD buffer	930 µL	960 µL
	Hypoxanthine	20 µL	20 µL
	Cytochrome c	10 µL	10 µL
	Sample	30 µL (?)	-
	Xanthine oxidase	10 µL	10 µL
TOTAL		1 mL	1 mL

Table 3.6. Composition of an example cuvette for SOD assay.

The amount of sample to put in cuvettes is determined empirically based on the % inhibition of the colorimetric reaction, calculated with the following formula:

$$\% \text{ inhibition} = 100 - [(A_S / A_B) \times 100]$$

A_B = Δ blank absorbance A_S = Δ sample absorbance

To have significant data, the percentage of inhibition of the assay must be between 40 and 60%, in this way we are sure to be in the part of the Lambert-Beer graph in which the relationship between absorbance and concentration is linear.

Absorbance was measured at a wavelength of 550 nm at 10 s intervals for a total time of 3 minutes per sample. For each sample, the change in absorbance of a corresponding blank was measured; with this, the difference in the increase in absorbance during the reaction was calculated. The absorbance delta was read in the 30 s (=0,5 min) interval having a

coefficient of determination (R^2) closest to 1 (the increase had the most linear trend possible). A maximum of three replicates were carried out for each sample, in order to have an experimental error of less than 15%. To minimize setup errors, blank and sample were read simultaneously.

- The concentration of SOD in the sample was measured, using the Lambert-Beer law:

$$(\text{U SOD/mL}) = [(A_B\text{-}A_S)/A_B] \,/0{,}5$$

- The result of the activity was multiplied by the sample dilution factor:

$$(\text{U SOD/mL}) \times 1/V_S \text{ (mL)}$$

- The result was divided by the total protein content of the sample, to normalize the SOD units to mg of total proteins:

$$\text{U SOD/mg di proteins} = \frac{(\text{U SOD/mL})}{(\text{mg proteins/mL})}$$

3.6.3. GPx ACTIVITY ASSAY

The GPx assay was carried out indirectly. The conversion of hydroperoxides by GPx uses GSH as a reducing factor, which oxidizes to GSSG. This reaction is coupled to the reduction of GSSG to GSH by GR, which uses NADPH as a reducing factor; this oxidizes to $NADP^+$, resulting in a change in color and consequent decrease in absorbance. The GPx activity, proportional to the decrease in NADPH, was then obtained by following the change in absorbance during the reaction kinetics, using a spectrophotometer. On the other hand, in the absence of GPx, NADPH is not oxidized; therefore, only a slight variation in absorbance is recorded, however less than the decrease observed in the presence of GPx. Hydrogen peroxide was used as the substrate; therefore, the activity of only selenium-dependent GPx was evaluated.

The following solutions were prepared:

- Stock solution: 0,0062 g of NADPH (0,15 mM) + 0,019 g of GSH (2,5 mM) + 0,002 g of NaN_3 (1,25 mM) + 52,5 µL of GR in 25 mL of phosphate buffer (125mM);
- H_2O_2 solution: 14 µL of stock H_2O_2 (30%) in 50 mL of H_2O (absorbance at 240 nm > 0,106).

Samples were analyzed in two replicates; a single blank was carried out for all measurements. Cuvettes were set up as in Table 3.7:

		SAMPLE	BLANK
REAGENTS	Stock solution	800 µL	800 µL
	Phosphate buffer	90 µL	100 µL
	Sample	10 µL	-
	H_2O_2 solution	100 µL	100 µL
TOTAL		1 mL	1 mL

Table 3.7. Composition of cuvettes for GPx assay.

The absorbance was read at a wavelength of 340 nm, at regular intervals of 60 s, for a total time of 300 s. The delta of absorbance in the total 5 minute trace was considered. GPx units per mg of total proteins were calculated as follows:

- The normalized absorbance variation on the blank was calculated:

$$\Delta = A\text{-}B$$

- The enzymatic activity of GPx was calculated with the Lambert-Beer law, per minute, per unit of volume:

$$\text{U GPx/mL} = \left[\frac{(Ai - Af)}{\Delta t/6{,}22}\right] \text{x} \frac{1000}{\text{V sample}}$$

- The result was normalized to the mg of total protein present in the sample:

$$\text{U GPx/mg proteins} = \frac{(\text{U GPx/mL})}{(\text{mg proteins/mL})}$$

3.6.4. CAT ACTIVITY ASSAY

Aebi (1984) method was used to quantify catalase activity. Catalase works by reducing hydrogen peroxide to water, to produce oxygen. The rapid decomposition of H_2O_2 can be deduced directly from the decrease in absorbance, read at a wavelength of 240 nm. The following solutions were prepared:

- Phosphate buffer Na_2HPO_4 – NaH_2PO_4 (50 mM, pH 7,5);
- H_2O_2 solution: 170 µl of stock H_2O_2 (30%) in 50 mL of H_2O (absorbance < 1,18).

Quartz cuvettes were set up with the following composition (Table 3.8):

		SAMPLE	BLANK
REAGENTS	Phosphate buffer	1970 µL	1970 µL
	Homogenization buffer	-	30 µL
	Sample	30 µL	-
	H_2O_2 solution	1000 µL	1000 µL
TOTAL		3 mL	3 mL

Table 3.8. Composition of cuvettes for CAT assay.

Enzymatic kinetics were followed every 5 seconds for a total time of 1 minute. For each sample 2 replicates were performed.

- The amount of active enzyme was calculated with the Lambert-Beer law; the value was multiplied by the dilution factor and normalized per minute:

$$\text{U CAT/mL} = \left[\frac{(\text{Ai} - \text{Af})}{40/0{,}833}\right] \text{x} \frac{\text{Total V}}{\text{V sample}} x\ 1000$$

- The amount of enzyme has been normalized on the amount of total proteins present in the sample:

$$\text{U CAT/mg proteins} = \frac{(\text{U CAT/mL})}{(\text{mg proteins/mL})}$$

3.6.5. AOPP DETERMINATION

Advanced Oxidation Protein Products (AOPP) were measured using the Witko-Sarsat spectrophotometric method (Witko-Sarsat et al. 1998) on a microplate reader. A calibration line was constructed with chloramine-T (N-chloro-p-toluenesulfonamide sodium salt), diluted in PBS at scalar concentrations from 0 to 100 µmoles/L, with a sensitivity of 3,125 µL. Chloramine-T in the presence of potassium iodide absorbs at a wavelength of 340 nm in a linear manner. On a 96-well plate, the solutions were loaded in duplicate, as follows in Table 3.9:

		STANDARD	BLANK	SAMPLES
REAGENTS	PBS	-	200 µL	160 µL
	Chloramine-T	200 µL	-	-
	Plasma	-	-	40 µL
	KI	10 µL	10 µL	-
	Acetic acid	20 µL	20 µL	20 µL

Table 3.9. Composition of plate for AOPP determination.

The concentration of AOPP is expressed as a micromoles/liter of chloramine-T equivalent. The result was multiplied by the dilution factor 5

(40 µL of sample in total 200 µL) and finally normalized on the total protein content in the sample:

$$\frac{\text{AOPP}}{\text{mg proteins}} = \frac{[\text{AOPP}] * \frac{200}{40}}{\text{mg proteins/mL}}$$

3.6.6. LIPID PEROXIDATION (MDA)

Lipid Peroxidation (MDA) Assay kit (Colorimetric/Fluorometric) was used to quantify lipid peroxidation. In this kit, lipid peroxidation is determined by the reaction of malondialdehyde (MDA) with thiobarbituric acid (TBA) to generate an MDA-TBA adduct; this can be quantified by colorimetric analysis, reading the absorbance at 532 nm, proportional to the concentration of MDA.

For this assay, a vial of TBA solution (250 mg) was reconstituted in 7,5 ml glacial acetic acid, then adjusted to 25 ml with ultrapure water and stored at 4 °C.

A standard curve was set up. A stock standard solution of MDA 0,1 M was prepared diluting 10 µL of the 4.17 MDA Standard Solution with 407 µL of ultrapure water. Further 20 µL of the 0.1 MDA Standard Solution was dilute with 980 µL of ultrapure water to prepare a 2 mM MDA Standard. The obtained solution was used to prepare MDA standards in 1,5 mL microcentrifuge tubes according to Table 3.10.

WELL	2 mM MDA STANDARD	ULTRAPURE WATER	MDA (nmol/well)
1	-	200 µL	0 nmol
2	2 µL	198 µL	4 nmol
3	4 µL	196 µL	8 nmol
4	6 µL	194 µL	12 nmol
5	8 µL	192 µL	16 nmol
6	10 µL	190 µL	20 nmol

Table 3.10. Standard curve preparation for LPO.

For each sample 10 mg of tissue were weighed, then washed with PBS buffer. 150 µL of ultrapure water and 3 µL of BHT were added to each sample. These were then vortexed and homogenized with pestles after the addition of 163 µL of 2N perchloric acid. Samples were briefly centrifuged to remove precipitated proteins. 110 µL of supernatant was collected from each sample into a new Eppendorf tube. To form the MDA-TBA adduct, 330 µL of TBA solution was added to Standard and Sample; these were then incubated at 95°C for 60 minutes and kept on ice for 10 minutes.

In a 96 well plate with clear flat bottom were loaded:

- Standard wells: 200 µL from the Standard Solution;
- Sample wells: 200 µL of supernatant containing MDA-TBA adduct.

Every well, both for standard and sample, was read in duplicate. The sample optical density (OD) was read on a spectrophotometer (microplate reader TECAN Infinite® F200PRO) at 532 nm.

The normalized absorbance was calculated subtracting the mean absorbance value of the blank from al the means of sample and standard readings. Background values can be significant and must be subtracted from all readings. The amount of MDA present in the samples may be determined from the standard curve. For each standard, the normalized absorbance was plotted against Standard concentrations of MDA, to obtain the linear equation and the slope of the standard curve. Using the standard curve, the quantity of MDA in nanomoles of each sample was determined. The concentration of MDA in the sample was then calculated as:

$$\text{Concentration of MDA (nmol/mL)} = \left(\frac{S_A}{S_V}\right) \text{ x DF}$$

Where:

- S_A: amount of MDA in sample (nmol) as determined from the standard curve;
- S_V: sample amount (mg) added into wells;
- DF: sample dilution factor.

3.7. STATISTIC ANALYSIS

The results have been shown as mean values ± SD (Standard Deviation). For the statistical analysis of the data, the Primer.exe program (Version 1.0, Stanton A. Glantz, Italy) was used. A one-way variance analysis (ANOVA) was applied, followed by the Student-Newman-Keuls test to determine the significance. A *p*-value < 0,05 was considered statistically significant.

4. RESULTS

4.1. GENE TRANSCRIPTION

The qRT-PCR analyses allowed the evaluation of gene expression at the transcriptional level of genes, coding for the following antioxidant enzymes: SOD, GPx, CAT and Prdx. The mRNA expression was evaluated for each gene in specimens sampled in the three previously described sampling sites.

4.1.1. *sod1* mRNA EXPRESSION

From the graph of Figure 4.1, it is possible to note a statistically significant increase ($p < 0.05$) in the level of *sod1* mRNA in the specimens from the "low polluted" site compared to the control site. In particular, the percentage increase is 288.9%. There is no significant variation in gene expression between the "highly polluted" site and the control site.

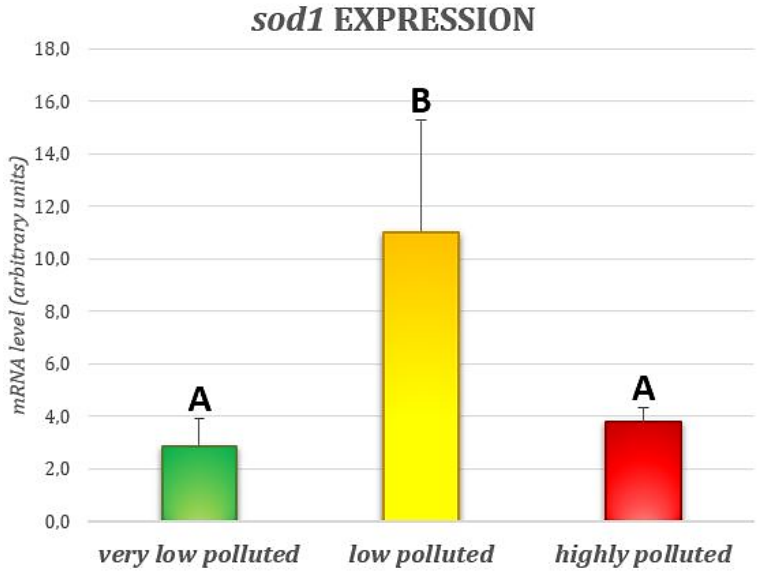

Figure 4.1. sod1 expression in mean values (N=8) with relative standard deviations. Different colours represent the three sites: "very low polluted site" in green, "low polluted site" in yellow, "highly polluted site" in red. Different letters in the graph indicate statistically significant differences ($p < 0.05$).

4.1.2. *sod2* mRNA EXPRESSION

The graph in Figure 4.2 shows a statistically significant increase ($p < 0.05$) in gene transcription of the *sod2* gene of the specimens from both the "low polluted" site and the "highly polluted" site compared to the control site (about 71% higher). There is no significant variation between the fish sampled in these two sites.

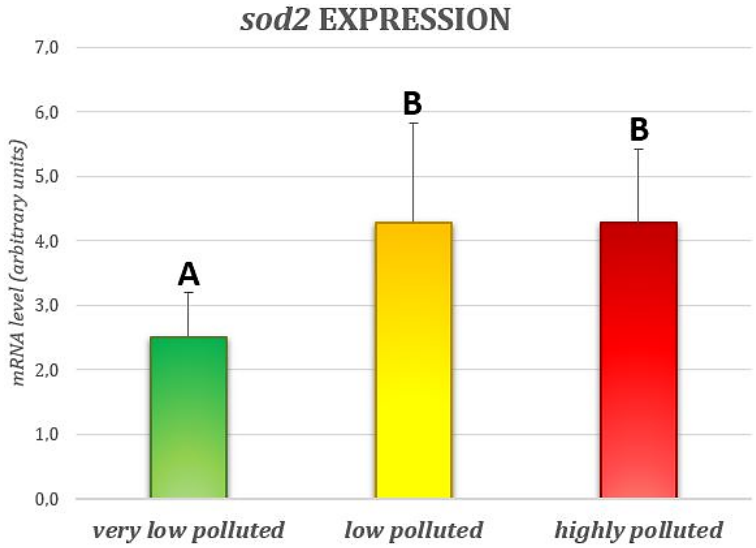

Figure 4.2. sod2 expression in mean values (N=8) with relative standard deviations. Different colours represent the three sites: "very low polluted site" in green, "low polluted site" in yellow, "highly polluted site" in red. Different letters in the graph indicate statistically significant differences ($p < 0.05$).

4.1.3. *gpx1* mRNA EXPRESSION

The graph in Figure 4.3 shows a statistically significant increase ($p < 0.05$) in the gene transcription of the *gpx1* gene in specimens sampled in the "highly polluted" compared to the control site. In particular, there was a 54.3% increase. No significant difference exists between the "low polluted" and control sites.

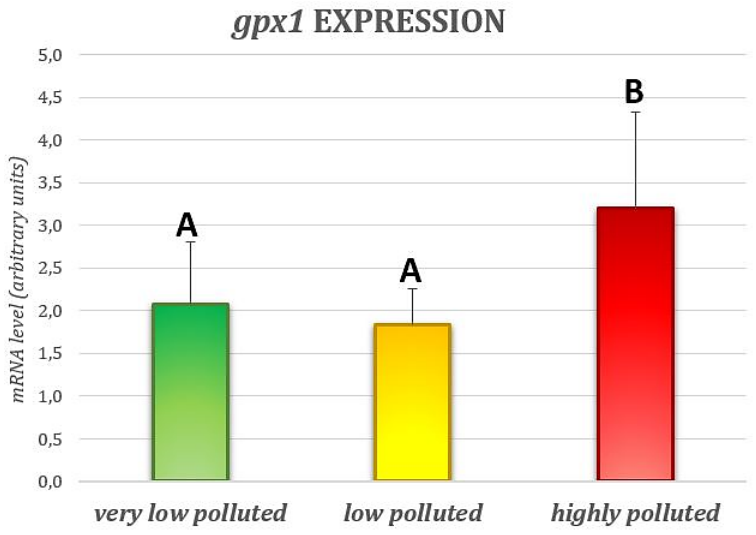

Figure 4.3. gpx1 expression in mean values (N=8) with relative standard deviations. Different colours represent the three sites: "very low polluted site" in green, "low polluted site" in yellow, "highly polluted site" in red. Different letters in the graph indicate statistically significant differences ($p < 0.05$).

4.1.4. *gpx4* mRNA EXPRESSION

The graph in Figure 4.4 shows a statistically significant increase ($p < 0.05$) in the transcription of the *gpx4* gene at the "low polluted" site compared to the control site. The percentage increase is 58%. No statistically significant variation exists between the "highly polluted" and control sites.

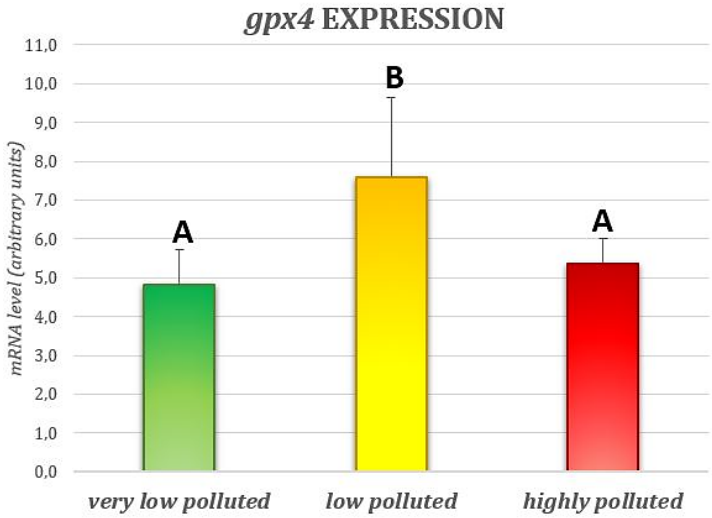

Figure 4.4. gpx4 expression in mean values (N=8) with relative standard deviations. Different colours represent the three sites: "very low polluted site" in green, "low polluted site" in yellow, "highly polluted site" in red. Different letters in the graph indicate statistically significant differences ($p < 0.05$).

4.1.5. *cat* mRNA EXPRESSION

No statistically significant differences in the *cat* gene expression levels were verified in the three sites (Figure 4.5).

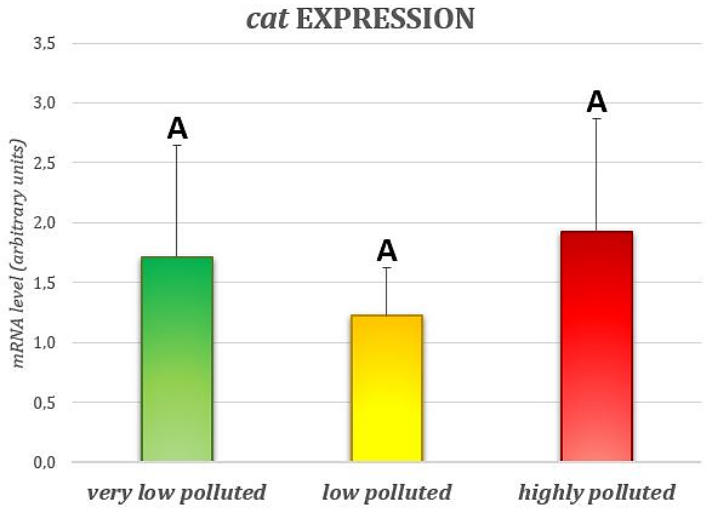

Figure 4.5. cat expression in mean values (N=8) with relative standard deviations. Different colours represent the three sites: "very low polluted site" in green, "low polluted site" in yellow, "highly polluted site" in red. Different letters in the graph indicate statistically significant differences ($p < 0.05$).

4.1.6. *prdx1* mRNA EXPRESSION

The graph in Figure 4.6 shows a statistically significant increase ($p < 0.05$) in the transcription of the *prdx1* gene both at the "low polluted" site and the "highly polluted" site compared to the control site. In particular, there is a percentage increase of 117.3% in specimens from the "low polluted" site and 134.1% from the "highly polluted" site. There is no significant difference between these two sites.

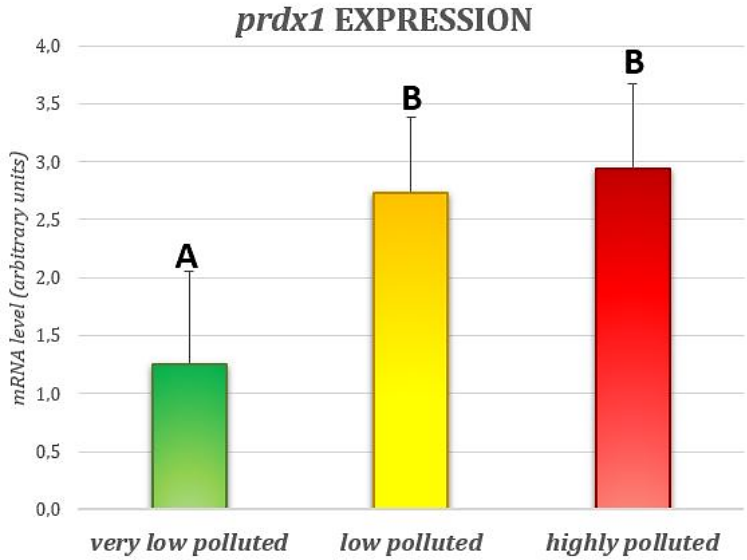

Figure 4.6. prdx1 expression in mean values (N=8) with relative standard deviations. Different colours represent the three sites: "very low polluted site" in green, "low polluted site" in yellow, "highly polluted site" in red. Different letters in the graph indicate statistically significant differences ($p < 0.05$).

4.1.7. *prdx2* mRNA EXPRESSION

Figure 4.7 shows a statistically significant increase ($p < 0.05$) in the mRNA level of the *prdx2* gene both at the "low polluted" site and at the "highly polluted" site compared to the control site. The extent of these increases is 170.5% for the chubs from the "low polluted" and 244.5% for the fish from the "highly polluted". There is no significant variation between these two sites.

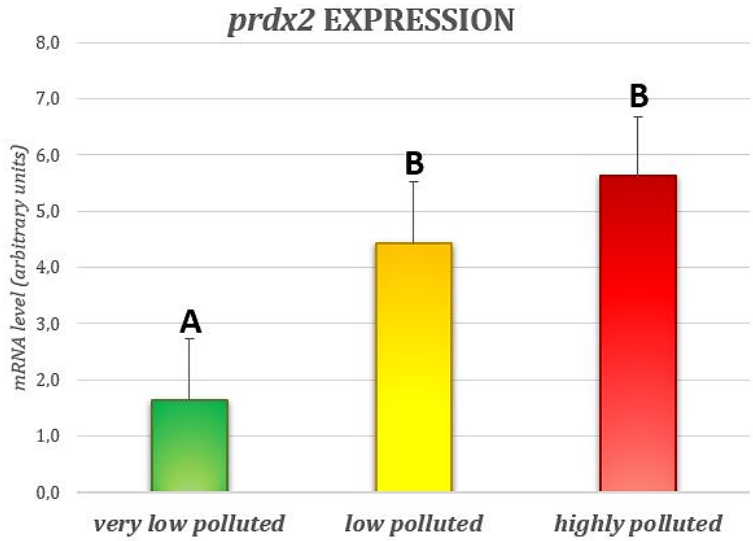

Figure 4.7. prdx2 expression in mean values (N=8) with relative standard deviations. Different colours represent the three sites: "very low polluted site" in green, "low polluted site" in yellow, "highly polluted site" in red. Different letters in the graph indicate statistically significant differences ($p < 0.05$).

4.1.8. *prdx3* mRNA EXPRESSION

The graph in Figure 4.8 shows a statistically significant increase ($p < 0.05$) in the mRNA expression of the *prdx3* gene in the "highly polluted" site compared to the control site. In particular, the percentage increase is 154.5%. No statistically significant variation exists between the "low polluted" and control sites.

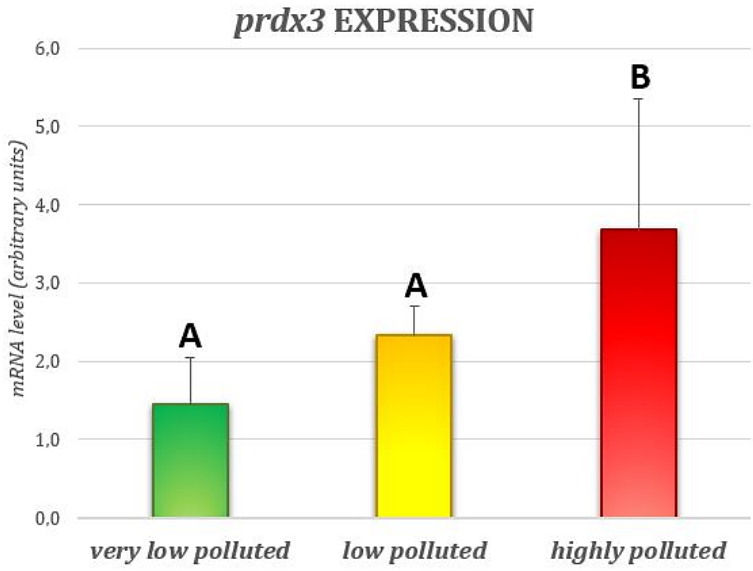

Figure 4.8. prdx3 expression in mean values (N=8) with relative standard deviations. Different colours represent the three sites: "very low polluted site" in green, "low polluted site" in yellow, "highly polluted site" in red. Different letters in the graph indicate statistically significant differences ($p < 0.05$).

4.1.9. *prdx4* mRNA EXPRESSION

Figure 4.9 shows a statistically significant ($p < 0.05$) decrease in mRNA levels of the *prdx4* gene both at the "low polluted" site and the "highly polluted" site compared to the control site. The decrease in these two sites is 58% and 63.1%, respectively. No significant variation exists between the "low polluted" and "highly polluted" sites.

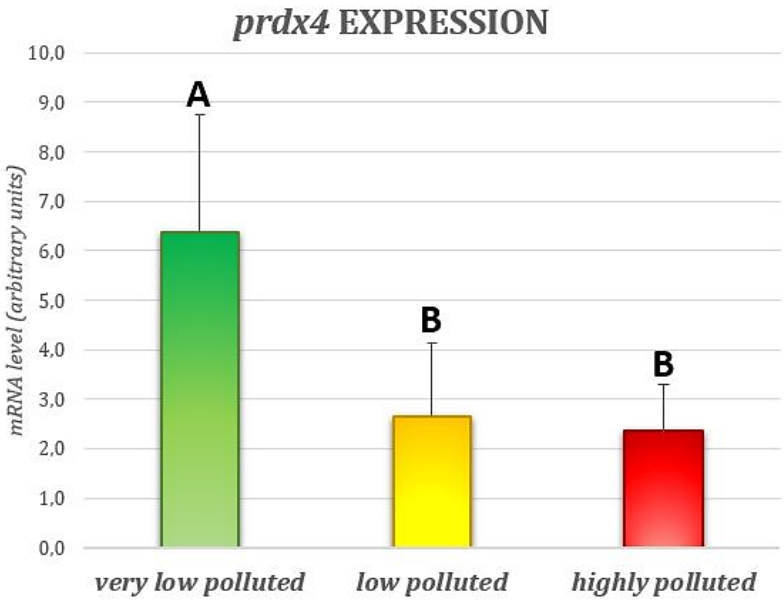

Figure 4.9. prdx4 expression in mean values (N=8) with relative standard deviations. Different colours represent the three sites: "very low polluted site" in green, "low polluted site" in yellow, "highly polluted site" in red. Different letters in the graph indicate statistically significant differences ($p < 0.05$).

4.1.10. *prdx5* mRNA EXPRESSION

The specimens from both the "low polluted" site and the "highly polluted" showed a statistically significant increase in the transcription of the *prdx5* gene compared to the control site (Figure 4.10). There is a 62.7% increase in the "low polluted" and a 48.9% increase in the "highly polluted" one. There is no significant variation between specimens from these two sites.

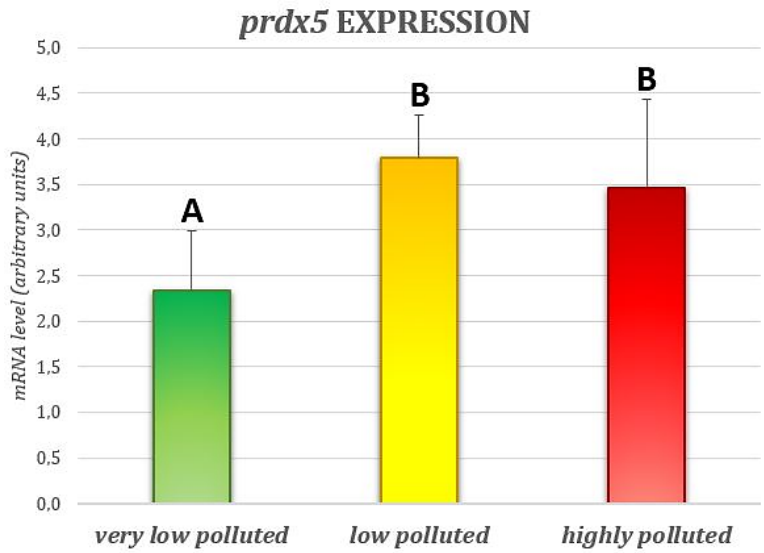

Figure 4.10. prdx5 expression in mean values (N=8) with relative standard deviations. Different colours represent the three sites: "very low polluted site" in green, "low polluted site" in yellow, "highly polluted site" in red. Different letters in the graph indicate statistically significant differences ($p < 0.05$).

4.1.11. *prdx6a* mRNA EXPRESSION

The graph in Figure 4.11 shows a statistically significant increase ($p < 0.05$) in the mRNA level of the *prdx6a* gene at the "low polluted" site compared to the control site. In particular, there was a 121.4% increase. No significant variation exists between specimens from the "highly polluted" and control sites.

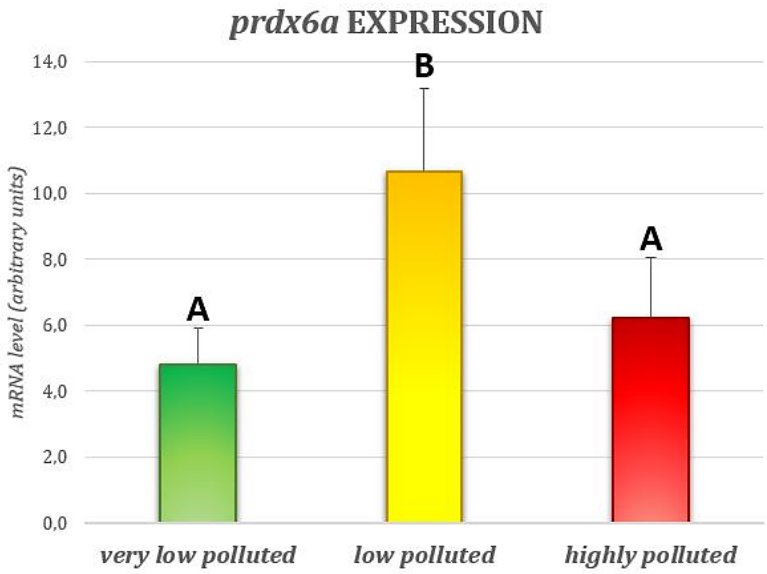

Figure 4.11. prdx6a expression in mean values (N=8) with relative standard deviations. Different colours represent the three sites: "very low polluted site" in green, "low polluted site" in yellow, "highly polluted site" in red. Different letters in the graph indicate statistically significant differences ($p < 0.05$).

4.2. ENZYMATIC TISSUE ACTIVITY

Specific biochemical assays have been applied to evaluate the amount of active antioxidant enzymes in the renal tissue. The analysed enzymes were: SOD, Se-GPx and CAT.

4.2.1. SOD ACTIVITY

The graph in Figure 4.12 shows a statistically significant increase ($p < 0.05$) in SOD activity in the kidney of specimens from both the "low polluted" site and the "highly polluted" site with respect to the control site. The increase is 51.1% and 37.7%, respectively. There is no significant difference between the animals sampled in these two sites.

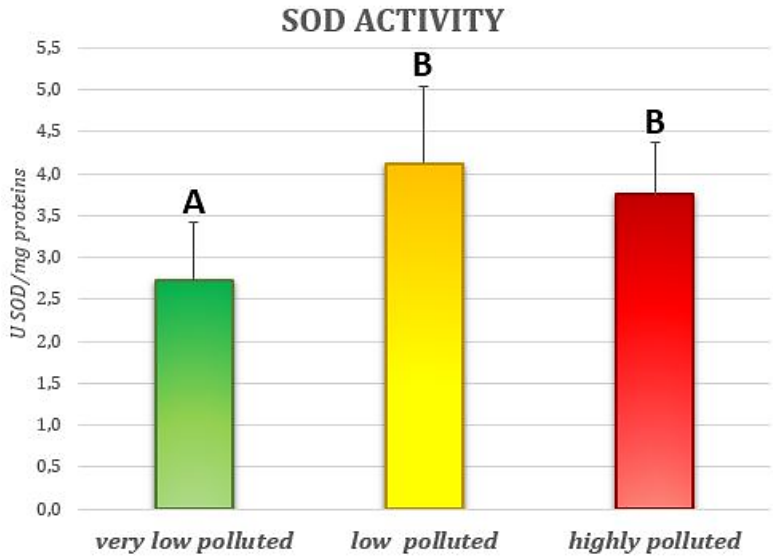

Figure 4.12. SOD activity (U SOD/mg proteins) in mean values (N=8) with relative standard deviations. Different colours represent the three sites: "very low polluted site" in green, "low polluted site" in yellow, "highly polluted site" in red. Different letters in the graph indicate statistically significant differences ($p < 0.05$).

4.2.2. Se-GPx ACTIVITY

The graph in Figure 4.13 shows a statistically significant increase ($p < 0.05$) in Se-GPx activity at the "highly polluted" site compared to the control site. In particular, there is a 75.2% increase. There is no significant difference between the activities measured in fish from the "low polluted" site and the control one.

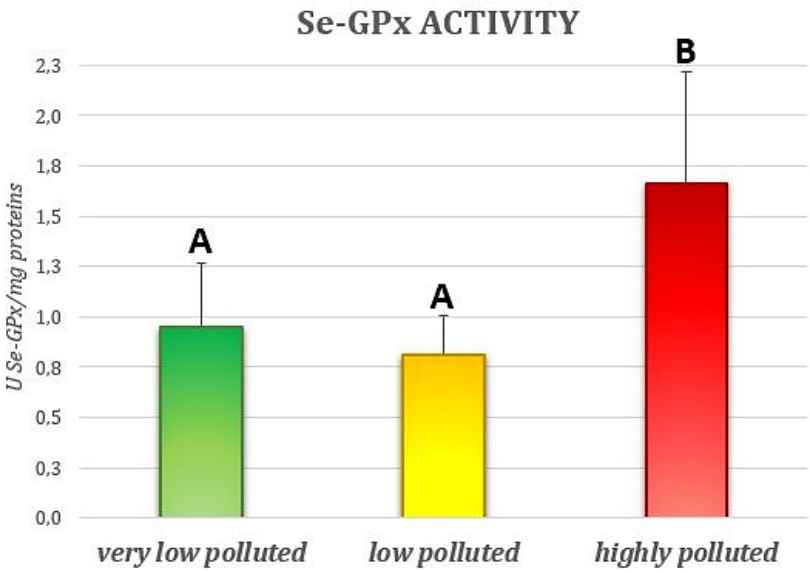

Figure 4.13. Se-GPx activity (U Se-GPx/mg proteins) in mean values (N=8) with relative standard deviations. Different colours represent the three sites: "very low polluted site" in green, "low polluted site" in yellow, "highly polluted site" in red. Different letters in the graph indicate statistically significant differences ($p < 0.05$).

4.2.3. CAT ACTIVITY

There is a statistically significant increase ($p < 0.05$) in catalase activity in specimens sampled in the "low polluted" site compared to those from the control site. The increase is of 55.2%. No significant change involves specimens from the "highly polluted" site.

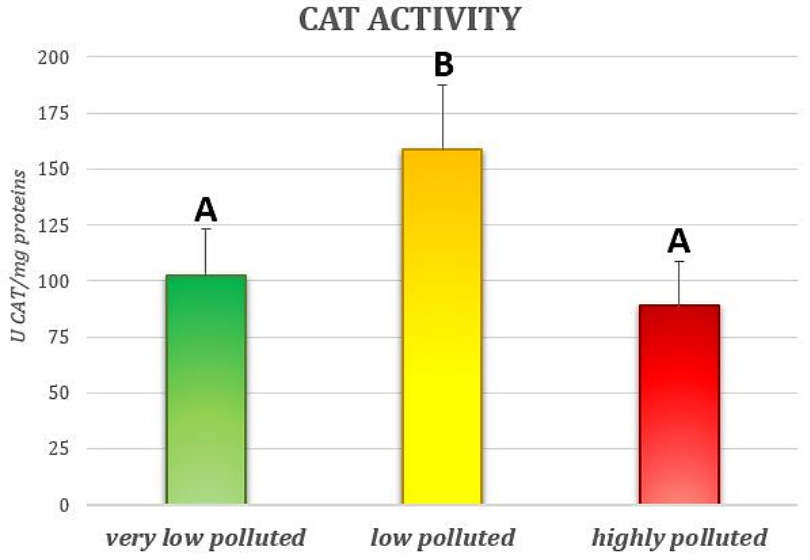

Figure 4.14. CAT activity (U CAT/mg proteins) in mean values (N=8) with relative standard deviations. Different colours represent the three sites: "very low polluted site" in green, "low polluted site" in yellow, "highly polluted site" in red. Different letters in the graph indicate statistically significant differences ($p < 0.05$).

4.3. INDICATORS OF OXIDATIVE CELL DAMAGE

Advanced Oxidation Protein Products (AOPP) and Lipid Peroxidation levels were evaluated as indicators of oxidative cell damage.

4.3.1. PROTEIN OXIDATION

The graph in Figure 4.15 shows a statistically significant increase ($p < 0.05$) in AOPP levels in the kidney of the specimens from both the "low polluted" site and the "highly polluted" site compared to the control site (about 47% higher).

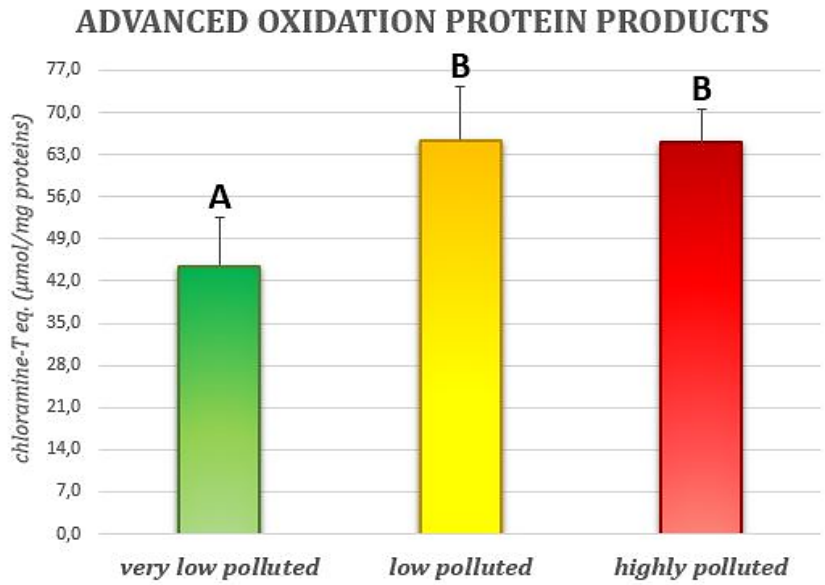

Figure 4.15. AOPP, expressed in chloramine-T eq. (µmol/mg proteins), in mean values (N=8) with relative standard deviations. Different colours represent the three sites: "very low polluted site" in green, "low polluted site" in yellow, "highly polluted site" in red. Different letters in the graph indicate statistically significant differences ($p < 0.05$).

4.3.2. LIPID PEROXIDATION

MDA levels measured in the kidney are not statistically different in the three sampling sites.

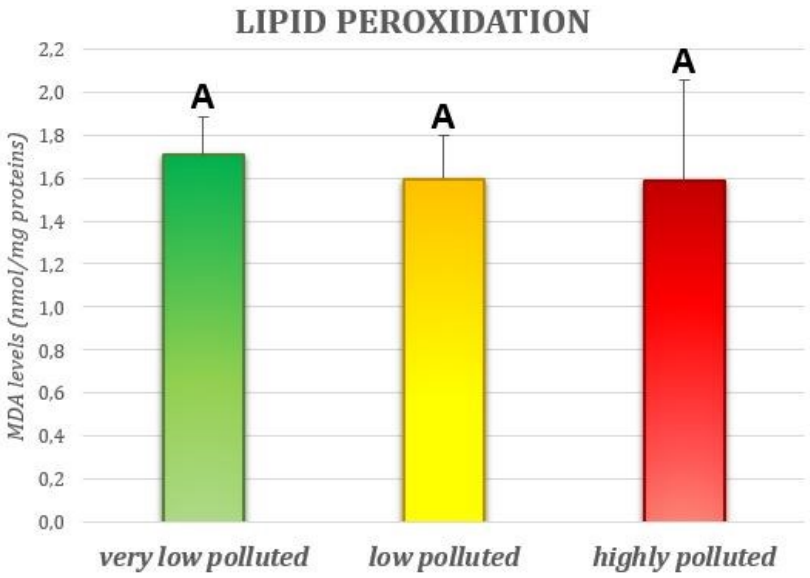

Figure 4.16. LPO expressed in MDA levels (nmol/mg proteins), in mean values (N=8) with relative standard deviations. Different colours represent the three sites: "very low polluted site" in green, "low polluted site" in yellow, "highly polluted site" in red. Different letters in the graph indicate statistically significant differences ($p < 0.05$).

5. DISCUSSION

For the present study, the rivers of the Veneto region represented an open-air laboratory since they offered variability in terms of PFAS concentration. In fact, the three sampling sites (Torrente Leogra, Roggia Moneghina, Retrone River) were selected for the different concentrations of these pollutants. Obviously, we cannot 100% rule out the possibility of other potential stress factors in environmental contamination. However, the sites were similar for other environmental parameters, such as temperature and other pollutants. In this way, although we have not evaluated the levels of PFAS bioaccumulation in the kidney, we can attribute any possible alteration of the physiological responses of the organisms to the different environmental PFAS concentrations.

The present work has sought to understand through multiple analyses how chronic environmental exposure to PFAS may increase the risk of oxidative stress in fish, particularly in the kidney of the species *Squalius cephalus*, chosen based on its wide diffusion, ubiquity and ability to live even in the most polluted waters. Studies on chub have already been carried out in our laboratory. In these, a variation in antioxidant responses was found in relation to PFAS exposure in other organs, such as liver, gills, gonads and spleen (Piva et al., 2022). Therefore, the obtained results enrich information regarding oxidative stress risk induced by PFAS and the physiological responses activated to counter it.

5.1. SUPEROXIDE DISMUTASE (SOD)

The induction of SOD does not seem to be dose-dependent. In fact, there is a significant increase in both mRNA expression and enzymatic activity in chub from the "low polluted" site, and there is no further increase in specimens from the most polluted site. From these results, it can be deduced that even a low concentration of PFAS can increase the rate of $\bullet O_2^-$ formation in the kidney. SODs are often cited as the first line of defence against oxygen-derived free radicals. They can be rapidly induced to inhibit oxidative damage in mitochondria stress in response to ROS formation (He et al., 2017). Bonato et al. (2020) reviewed outcomes reported in environmental models, noting that exposure to PFAS leads to a generalised increase in SOD activity.

The absence of a further increase of SOD activation in specimens from the "highly polluted" site may be related to the chronic exposure condition of fish. We cannot exclude those organisms, at the first moments of exposure to an increased concentration of PFAS, have further increased SOD

biosynthesis to higher levels to respond to the increase in $\bullet O_2^-$ formation. Assuming a negative feedback control, typical of the antioxidant system, we can deduce that later, organisms have potentially found a balance such that greater production of SOD is still needed, but not as high as in the early stages of exposure, having restored the presence of $\bullet O_2^-$ back to almost physiological levels.

However, it is clear that this only partially returns to baseline values. There is a continuous production of $\bullet O_2^-$ due to the persistent presence of PFAS, but these appear to be effectively counteracted by the SOD levels we measured. The data also suggest that organisms are not yet under oxidative stress. In fact, their physiology is still able to counteract potential toxicity caused by PFAS exposure effectively. In a situation of oxidative stress, organisms would not even be able to increase the biosynthesis of antioxidant enzymes; in this case, the results should have shown a decrease in active enzyme biosynthesis.

The SOD activity assay made it possible to assess the total amount of enzyme present in the samples. However, it did not provide enough information to understand which isoform of SOD contributed most to the total activity and, thus, also which part of the cell is most involved in the increased superoxide radical formation. Indeed, the SOD1 isoform has a cytoplasmic localisation, while SOD2 acts at the mitochondrial level. This was helped by evaluating the expression of the *sod1* and *sod2* genes. The results showed a statistically significant increase in SOD1 mRNA accumulation exclusively at the "low polluted" site, whereas SOD2 gene transcription increased at both sites. We can deduce that low PFAS concentrations result in the development of $\bullet O_2^-$ in both the cytoplasm and the mitochondria, to which organisms respond by activating the transcription of both SOD isoforms.

These results are in line with expectations. In fact, mitochondria are the main intracellular organelles targeted by PFAS. Given the high affinity of perfluoroalkyl substances for proteins, they could interact with the enzymes involved in ETC, causing abnormal production of ROS. Given their short half-life, they would act mainly at the production site, i.e., the mitochondria, increasing the demand for SOD2. SOD1 activation at low PFAS concentrations could be a preventative response but sufficient to counteract a reduced increase in $\bullet O_2^-$.

The lack of SOD1 activation at high PFAS concentrations could be due either to a failure to produce superoxide radicals at the cytoplasmic level or to the activation of non-enzymatic antioxidants, such as GSH or MT, which could promote the nonspecific elimination of $\bullet O_2^-$. On the other hand,

scavenger action by other antioxidant enzymes is not plausible because they cannot specifically eliminate the $\bullet O_2^-$.

5.2. GLUTATHIONE PEROXIDASE (GPx)

The GPx enzyme assay showed an increase in Se-GPxs activity, from which we infer an increase in their biosynthesis, only at high concentrations of PFAS but not at low PFAS concentrations. Since GPx exerts its antioxidant action on H_2O_2 and organic peroxides, it can be concluded that high PFAS concentrations definitely produce these molecules, which is effectively counteracted by the scavenger action of GPx.

H_2O_2 could be formed directly from the dielectronic reduction of oxygen. Still, it is presumable that at least part of it derives from increased SOD activity itself, as in the case of the specimens sampled at the "highly polluted" site. In this case, GPx would act synergistically with SOD to limit the risk of oxidative stress.

However, as in the case of the SOD assay, it was not possible to discriminate the induction of the different isoforms of GPx, which act in different cellular compartments. Therefore, a gene expression analysis of the *gpx1* and *gpx4*, which code for cytoplasmic-localized GPx1 and mitochondrial-localized GPx4, respectively, was performed to assess the involvement of different isoforms. The results show a statistically significant increase in the expression of *gpx1* in the "highly polluted" site but not in the "low polluted". An opposite trend concerns the expression of *gpx4*, which increased in the "low polluted" site but not in the "highly polluted".

The data suggest that high concentrations of PFAS result in the development of peroxides at the cytoplasmic level, effectively counteracted by GPx1. However, we cannot exclude that other GPx isoforms may be involved in the antioxidant action against peroxides at the cytoplasmic level. Further gene expression analysis of other Se-GPx, such as GPx2 and GPx3, would be necessary.

The "low polluted" site presents a more particular situation. An increase in the total activity of Se-GPx does not accompany the rise in *gpx4* expression. Based on these data, it is evident that there is a post-transcriptional regulation that blocks the translation of the *gpx4* transcripts. The increase in mRNA for the mitochondrial isoform could thus represent a preventive response against the increased risk of oxidative stress due to PFAS exposure. Still, the translation of these messengers could occur only later, in case the need arises to implement antioxidant defences in mitochondria,

without necessarily immediately investing metabolic energy in the biosynthesis of this enzyme.

Stress granules may be involved in this regulatory process. They are membrane-free cytoplasmic foci, consisting of a pool of untranslated messengers blocked in the early phase of translation and containing various translation initiation factors, a variety of RNA-binding proteins, and many non-RNA-binding proteins (Protter and Parker, 2016). Organisms are usually exposed to environmental variability that can result in a potential stress situation, exerting this regulation to accelerate anti-stress responses. In fact, thanks to the stress granules, the cell can bypass the gene transcription step and start directly with the translation of an already present messenger. As long as the stress granules are not broken up, the messenger is protected from degradation but cannot be translated. When concentrations of granule components, such as untranslatable RNA, are high, ATPases transiently disrupt such interactions and thus help speed up exchange rates (Protter and Parker, 2016), making transcripts available for translation. The fact that the analysed organisms are not exposed to acute but chronic stress would justify the presence of stress granules. Of course, this statement remains only a hypothesis; to verify the presence or absence of these aggregates, it would be appropriate to evaluate the gene expression of some proteins involved in stress granule assembly. These include T cell intracellular antigen 1 (TIA1), RAS GTP-activating protein-binding protein 1 (G3BP1), TIA1-related protein (TIAR), tristetraprolin (TTP) (Wolozin and Ivanov, 2019). In a situation of reduced risk of stress, as in the "low polluted" site, one would expect increased expression of these proteins, associated with the observed increase in mRNA level of antioxidant enzymes such as GPx4 and reduced protein biosynthesis. Conversely, in a high-stress situation, one would expect an opposite trend, with a reduction in their expression, making the transcripts more available for translation.

5.3. CATALASE (CAT)

The results show a statistically significant increase in CAT activity in the specimens sampled at the "low polluted" site, compared to a non-significant difference between the "highly polluted" site and the control site. This result suggests that catalase can play a preventive action against oxidative stress at low PFAS concentrations, representing a first line of defence against increased H_2O_2. Since the primary localisation of CAT is at the level of the peroxisomes, we can also infer that the increased production of H_2O_2 involves these organelles. Exposure to higher PFAS concentrations results in a downregulation of CAT and, as we have seen, the entry into play of

other peroxidase enzymes, such as GPxs, which would represent the second line of defence against oxidative stress.

Analysis of CAT gene transcription shows, as with GPx, an apparently abnormal trend unrelated to enzyme activity. But here, too, the involvement of the regulation of expression driven by stress granules may explain these trends. Therefore, the increase in CAT activity in the "low polluted" site would not be due to activation of the *cat* gene. Still, the translation of its messengers was previously transcribed and stored within the stress granules.

5.4. PEROXIREDOXINS (Prdx)

Unfortunately, it was not possible to analyse the total peroxiredoxin activity. The method is rather complex, and unfortunately, a commercial kit is no longer available. However, evaluating the gene transcription of the various isoforms was possible, which gave interesting information. The results showed a complex and articulated antioxidant response involving peroxiredoxins, with up-regulation and down-regulation involving single genes.

In particular, there is an increase in *prdx3* transcription only at high PFAS concentrations. Prdx3 is specifically expressed at the mitochondrial level (Valero et al. 2015), and its induction following PFAS exposure was expected since, as we have already mentioned, mitochondria are a primary target for the toxicity exerted by these pollutants. The fact that messenger accumulation does not increase already at low environmental concentrations of PFAS leads us to believe that this antioxidant enzyme is part of the second line of defence against mitochondrial oxidative stress, coming into play after GPx4 induction. Delayed activation of the prdx3 gene has been verified in other fish species exposed to other sources of stress, such as an acute increase in temperature (Tolomeo et al., 2019).

In contrast, the other Prdx expressed in mitochondria, isoform 5, is induced already at low environmental PFAS concentrations, but its gene transcription is not necessarily directly related to mitochondria protection. In fact, Prdx5 can be considered a 'multitasking' protector, being also expressed at the cytoplasmic and peroxisomal levels (Valero et al., 2015) and as such, involved early on in the anti-stress response. Precisely, its expression in peroxisomes would confirm that these organelles are affected early on by increased H_2O_2 formation, as previously hypothesised based on CAT results.

Prdx1 and Prdx2 can also be considered multifunctional, as they are expressed in the cytoplasm, peroxisomes, nucleus, and plasma membrane (Valero et al., 2015). Thus, an increase in transcription of their genes was widely expected already at low environmental PFAS concentrations.

An interesting result concerns the gene expression of Prdx6a. This enzyme carries out its antioxidant action specifically in lysosomes (Valero et al., 2015), one of the targets of PFAS toxicity. In fact, these substances can induce a marked destabilisation of lysosomal membranes (Fabrello et al., 2021). Therefore, the increase in *prdx6a* gene transcription could nominate this isoform of Prdxs as the first line of defence in the antioxidant protection of these organelles. However, one would expect this induction to be maintained even after further increased environmental PFAS concentrations, which is not apparent from our data. However, it is known that a b-variant of Prdx6 also exists in fish, which has been shown to play the role of a second line of defence in fish exposed to heat stress (Tolomeo et al., 2016). Further analyses will be necessary to confirm that Prdx6a and Prdx6b could be alternately activated in response to different PFAS concentrations in the chub kidney.

Another very interesting result concerns the expression of prdx4. The results show a down-regulation of this isoform despite the increase in the environmental concentration of PFAS. A superficial assessment of this result might suggest that Prdx4 is less critical in antioxidant protection in the case of PFAS exposure. Prdx4 is specifically expressed in the endoplasmic reticulum (Valero et al., 2015), where it acts as a scavenger against peroxides but also has the function of inhibiting lipid accumulation in the cell (Yamada and Guo, 2018). Previous studies have verified that in the fish species *Padogobius bonelli,* there is a positive correlation between lipid vacuolisation (steatosis) and PFAS accumulation in hepatocytes. The lipid accumulation could be considered a defence mechanism against the toxic effects of PFAS. In fact, it is known that these compounds show their toxicity against cytoplasmic proteins, which are purely hydrophilic molecules. By increasing the amount of fat inside the cell, the hydrophilicity of the intracellular environment is reduced, making the interaction between PFAS and the protein component less probable. By down-regulating the prdx4 gene, the inhibition of cellular lipid accumulation would be blocked, initiating the vacuolisation process.

A positive correlation between vacuolisation and PFAS accumulation in the liver was also shown in eels exposed to PFOA (Wolf and Wolfe, 2005), zebrafish exposed to PFOS (Du et al., 2017), and rats exposed to PFOA and PFOS (Harper and Wolf, 2009), but not in *S. cephalus* (Piva et al., 2022). However, it must be considered that only the liver was histologically

analysed in this species, so we cannot exclude the possibility of steatosis involving the kidney instead.

5.5. LIPID PEROXIDATION

No statistically significant differences were found between the "highly polluted" and the "low polluted" sites compared to the control sites. These data suggest that activation of the antioxidant defences previously described effectively protects the kidney from oxidative lipid damage.

Data from the literature show results that only sometimes concur. Some studies confirm the absence of lipid peroxidation despite exposure to PFAS. In fact, a decrease in lipid damage was highlighted in zebrafish liver and larvae after exposure to F–53B (Wu et al., 2019). In songbird (*Parus major*) exposed to PFAS, malondialdehyde levels did not differ among various sites examined, suggesting that lipid peroxidation was unaffected (Buytaert et al., 2023). Other studies show an increase in lipid peroxidation due to PFAS exposure. Several in vivo and in vitro studies have indicated that PFAS, including PFOS and PFOA, can induce oxidative stress, evidenced by an increase in ROS production and increased lipid peroxidation (Ojo et al., 2021). Another study showed that higher levels of PFAS were associated with increased levels of oxidative stress evidenced using biomarkers such as protein oxidation, DNA damage, and lipid peroxidation (Chen et al., 2023).

It is essential to consider that the analysed individuals were chronically exposed to PFAS in our case. It cannot be ruled out that during the acute phase of exposure, they experienced an increase in lipid oxidation. Still, later, by activating antioxidant gene system defences, they may have reached a new equilibrium characterised by the absence of lipid peroxidation in the kidney, as already verified in the liver (Piva et al., 2022).

Our study demonstrates an activation of the antioxidant enzyme system, which can eliminate ROS before they damage membrane lipids. However, the available data do not allow us to clearly exclude the possible initial oxidation of lipids and the possible intervention of other non-enzymatic, chain-breaking antioxidants such as GSH and vitamins. Therefore, it would be interesting to clarify this hypothesis by quantifying the concentrations of these molecules in the kidney.

Antioxidant systems counter oxidation in two ways: protecting target lipids from oxidation initiators or blocking the propagation phase of oxidative damage. In the first case, so-called preventive antioxidants hinder the formation of ROS or scavenge the species responsible for initiating

oxidation ($\bullet O_2^-$, $^1O_2$). In the second case, so-called "chain-breaking" antioxidants intercept the propagators of radical oxidation (LOO•) or participate indirectly in stopping the propagation of radical chains (Laguerre et al., 2007).

Our study demonstrates an activation of the antioxidant enzyme system, which can eliminate ROS before they damage membrane lipids. However, the available data do not allow us to clearly exclude the possible initial oxidation of lipids and the possible intervention of other non-enzymatic, chain-breaking antioxidants such as GSH and vitamins. Therefore, it would be interesting to clarify this hypothesis by quantifying the concentrations of these molecules in the kidney.

5.6. ADVANCED OXIDATION PROTEIN PRODUCTS

The AOPP assay shows an entirely different trend than lipid peroxidation. There was a statistically significant increase in protein oxidation at both the "low polluted site" and the "highly polluted" one compared to the control site. Therefore, the results show that even low PFAS concentrations are sufficient to promote the formation of ROS that cause oxidative damage to proteins and that the damage remains even in chronic exposure conditions.

It is well known that at the same concentration of ROS, the target substrate most affected by the increased risk of oxidative stress due to PFAS exposure are proteins rather than lipids. In birds, a correlation was found between higher oxidative protein damage and higher concentrations of perfluorododecanoic acid (PFDoA), perfluorotridecanoic acid (PFTriA) and perfluorotetradecanoic acid (PFTeA) (Costantini et al., 2019). Since PFAS interact more with proteins, it is plausible that the latter include enzymes involved in cellular oxidoreductive systems, resulting in altered ROS production. Given their short half-life, it is conceivable that ROS oxidise primarily on the first molecules they encounter, i.e. the proteins themselves.

However, although significantly increased protein damage is present in the specimens analysed, it is equally evident that the fish studied are healthy, probably because maintaining high levels of antioxidant defences avoids even more significant molecular damage. Obviously, this requires an extra investment of metabolic energy, with possible consequences for the life history of these fish.

6. CONCLUSIONS

The present study investigated the possible toxicity of PFAS to organisms at the level of the antioxidant system. This research confirmed that PFAS can increase the risk of oxidative stress in the kidney, triggering the activation of some physiological responses. In particular, not only punctual events that acutely expose organisms to PFAS pose a risk to the ecosystem, but also the chronic presence of these substances in watercourses, which thus merits further investigation.

The kidney uses multiple systems to eliminate PFAS; some are ATP-dependent carriers (Niu et al., 2023). More significant PFAS accumulation requires higher kidney activity and increases metabolic energy demand. The enhanced ATP production determines a greater increase in ROS production by the mitochondrial ETC and the risk of oxidative stress.

It was observed that PFAS can cause damage to proteins, increasing their oxidation but not to lipids, leaving their peroxidation unaltered. However, fish try to contrast this effect by activating different antioxidant defences at various cellular compartments and in the extracellular matrix.

Chub showed modulation of the antioxidant defences, with up-and down-regulation of different genes in the intracellular location in which PFAS perform a more significant adverse action through the production of ROS. Thus, there isn't a quantitative response, with an indiscriminate increase of all defences, but a qualitative one, with activation and inactivation of different gene systems, in some cases related to the variability of PFAS concentrations. Fish often showed an alternative action of GPx and CAT to eliminate hydrogen peroxide. The down-regulation of some isoforms of the same enzyme represents a strategy to avoid transcription of less valuable isoforms, saving metabolic energy, which can help implement the action of other antioxidant system components.

The physiological responses to PFAS are complex; they include variation at transcriptional and post-transcriptional levels. This study showed the hypothesized involvement of stress granules in response to PFAS contamination, but further research is necessary to understand this aspect. Valuable insights could consist of gene expression analyses for proteins involved in stress granules formation, such as TIAR or TTP; TEM microscopic analyses to verify anomalous protein accumulations in the cytoplasm; use an immunolabeling with fluorescent antibodies for these proteins.

This study provided analyses of SOD, GPx and CAT activities; a future Prdx assay is necessary to obtain a more complete picture of all antioxidant

enzymes activities. Evaluating GSH content and GST activity represents another future perspective to understand which defence is more involved in preventing lipid peroxidation. In future, gene expression for other GPx isoforms and *prdx6b* could be evaluated to clarify the statements of this study.

There is very little information about the gene sequences of *Squalius cephalus* antioxidant enzymes; it would be helpful to carry out a gene characterization to obtain the sequences and phylogenetic analyses to study the evolution of these enzymes. In this context, we have already obtained some partial coding sequences.

In this research, we assumed that PFAS were the contaminants mainly present in the three sites; however, there can be no absolute certainty. For this reason, it will be appropriate to perform exposure experiments with these fish in controlled laboratory conditions in the future.

In conclusion, this study potentially explains that PFAS contamination in the Veneto region represents an evident risk for organisms and other stressful factors. PFAS causes an increase in the risk of oxidative stress, but the oxidative stress condition in the kidney is avoided because chub physiology can respond at this level of PFAS contamination.

Recent measurements by ARPAV showed higher PFAS concentrations in other Veneto rivers (ARPAV, 2023), representing a risk for many aquatic organisms, higher than for chub, a generalist species capable of living in highly contaminated waters. Other less adapted species could not efficiently respond to PFAS contamination, and these pollutants could potentially be a higher danger for them. Therefore, a future scenario of water purification from these substances is necessary to avoid risks for all species present in the watercourses of the Veneto region.

7. BIBLIOGRAPHY

Agenzia Regionale per la Prevenzione e Protezione Ambientale del Veneto [ARPAV] (2023). Concentrazione di sostanze perfluoroalchiliche (PFAS) nelle acque prelevate da ARPAV.

Agenzia Regionale per la Prevenzione e Protezione Ambientale del Veneto [ARPAV] (2016). Sostanze perfluoroalchiliche, analisi sulle fonti di pressione ambientale, collettore consortile ARICA, sistema dei cinque depuratori ditta MITENI S.p.A.

Ahrens, L., & Bundschuh, M. (2014). Fate and effects of poly- and perfluoroalkyl substances in the aquatic environment: A review. *Environmental Toxicology and Chemistry*, 33(9), 1921–1929.

Alfano, M., & Cavazza, C. (2020). Structure, function, and biosynthesis of nickel-dependent enzymes. *Protein Science*, 29(5), 1071–1089.

Aruoma, O. I. (1998). Free radicals, oxidative stress, and antioxidants in human health and disease. *Journal of the American Oil Chemists' Society*, 75(2), 199–212.

Balestrieri, A., Prigioni, C., Remonti, L., Sgrosso, S., & Priore, G. (2006). Feeding ecology of *Leuciscus cephalus* and *Rutilus rubilio* in southern Italy. *Journal of Zoology*, 73(2), 129–135.

Banks, R.E., Smart, B. E., & Tatlow, J. C. (1994). Organofluorine chemistry: principles and commercial applications. *New York (NY): Plenum*, p. 670.

Barber, J. L., Berger, U., Chaemfa, C., Huber, S., Jahnke, A., Temme, C., & Jones, K. C. (2007). Analysis of per- and polyfluorinated alkyl substances in air samples from Northwest Europe. *Journal of Environmental Monitoring*, *9*(6), 530–541.

Bonato, M., Corrà, F., Bellio, M., Guidolin, L., Tallandini, L., Irato, P., & Santovito, G. (2020). PFAS Environmental Pollution and Antioxidant Responses: An Overview of the Impact on Human Field. *International Journal of Environmental Research and Public Health*, 17(21), 8020.

Brooke, D., Footitt, A., & Nwaogu, T. A. (2004). Environmental risk evaluation report: Perfluorooctane sulphonate (PFOS). *UK Environment Agency*.

Brumovský, M., Karásková, P., Borghini, M., & Nizzetto, L. (2016). Per- and polyfluoroalkyl substances in the Western Mediterranean Sea waters. *Chemosphere*, 159, 308–316.

Buck, R. C., Franklin, J., Berger, U., Conder, J. M., Cousins, I. T., de Voogt, P., Jensen, A. A., Kannan, K., Mabury, S. A., & van Leeuwen, S. P. (2011). Perfluoroalkyl and polyfluoroalkyl substances in the environment: Terminology, classification, and origins. *Integrated Environmental Assessment and Management*, *7*(4), 513–541.

Butt, C. M., Muir, D. C. G., & Mabury, S. A. (2014). Biotransformation pathways of fluorotelomer-based polyfluoroalkyl substances: A review. *Environmental Toxicology and Chemistry*, 33(2), 243–267.

Candas, D., & Li, J. J. (2014). MnSOD in Oxidative Stress Response-Potential Regulation via Mitochondrial Protein Influx. *Antioxidants & Redox Signaling*, 20(10), 1599–1617.

Cordiano, V. & Gentilini, P., BIO, Mondo (2019). PFAS: l'ennesimo disastro che non risparmia neppure la Toscana.

Du, J., Cai, J., Wang, S., & You, H. (2017). Oxidative stress and apotosis to zebrafish (*Danio rerio*) embryos exposed to perfluorooctane sulfonate (PFOS) and ZnO nanoparticles. *International Journal of Occupational Medicine and Environmental Health*, *30*(2), 213–229.

Espinosa-Diez, C., Miguel, V., Mennerich, D., Kietzmann, T., Sánchez-Pérez, P., Cadenas, S., & Lamas, S. (2015). Antioxidant responses and cellular adjustments to oxidative stress. *Redox Biology*, 6, 183–197.

European Food Safety Authority [EFSA] (2008). Perfluorooctanesulfonate (PFOS), perfluorooctanoic acid (PFOA) and their salts - Scientific Opinion of the Panel on Contaminants in the Food Chain". *The EFSA Journal*, 653: 1-131.

European Food Safety Authority [EFSA] (2011). Results of the monitoring of perfluoroalkylated substances in food in the period 2000-2009. *The EFSA Journal*, 9 (2): 2016, 1-34.

Fabrello, J., Targhetta, F., Ciscato, M., Asnicar, D., Bernardini, I., Milan, M., Patarnello, T., Marin, M. G., & Matozzo, V. (2021). First Evidence of In Vitro Effects of C6O4—A Substitute of PFOA—On Haemocytes of the Clam *Ruditapes philippinarum*. *Toxics*, *9*(8), Articolo 8.

Flohé, L., Toppo, S., & Orian, L. (2022). The glutathione peroxidase family: Discoveries and mechanism. *Free Radical Biology and Medicine*, 187, 113–122.

Ghifari, A. S., Saha, S., & Murcha, M. W. (2023). The biogenesis and regulation of the plant oxidative phosphorylation system. *Plant Physiology*, 192(2), 728–747.

Gregory, E. M., & Fridovich, I. (1973). Oxygen Toxicity and the Superoxide Dismutase. *Journal of Bacteriology*, 114(3), 1193–1197.

Harper, C., & Wolf, J. C. (2009). Morphologic Effects of the Stress Response in Fish. *ILAR Journal*, *50*(4), 387–396.

Hasler, J. A., Estabrook, R., Murray, M., Pikuleva, I., Waterman, M., Capdevila, J., Holla, V., Helvig, C., Falck, J. R., Farrell, G., Kaminsky, L. S., Spivack, S. D., Boitier, E., & Beaune, P. (1999). Human cytochromes P450. *Molecular Aspects of Medicine*, *20*(1), 1–137.

He, L., He, T., Farrar, S., Ji, L., Liu, T., & Ma, X. (2017). Antioxidants Maintain Cellular Redox Homeostasis by Elimination of Reactive Oxygen Species. *Cellular Physiology and Biochemistry*, *44*(2), 532–553.

Henry, B. J., Carlin, J. P., Hammerschmidt, J. A., Buck, R. C., Buxton, L. W., Fiedler, H., Seed, J., & Hernandez, O. (2018). A critical review of the application of polymer of low concern and regulatory criteria to fluoropolymers: Fluoropolymers PLC. *Integrated Environmental Assessment and Management*, 14(3), 316–334.

Jahnke, A., Barber, J. L., Jones, K. C., & Temme, C. (2009). Quantitative trace analysis of polyfluorinated alkyl substances (PFAS) in ambient air samples from Mace Head (Ireland): A method intercomparison. *Atmospheric Environment*, *43*(4), 844–850.

Jamdhade, A. R., Sunkar, R., & Hivrale, V. K. (2017). Zymographic Method for Distinguishing Different Classes of Superoxide Dismutases in Plants. *Plant Stress Tolerance: Methods and Protocols* (pp. 221–227).

Izawa, S., Inoue, Y., & Kimura, A. (1996). Importance of catalase in the adaptive response to hydrogen peroxide: Analysis of acatalasaemic *Saccharomyces cerevisiae*. *Biochemical Journal*, 320(1), 61–67.

Jomova, K., Raptova, R., Alomar, S. Y., Alwasel, S. H., Nepovimova, E., Kuca, K., & Valko, M. (2023). Reactive oxygen species, toxicity, oxidative stress, and antioxidants: Chronic diseases and aging. *Archives of Toxicology*, *97*(10), 2499–2574.

Kirkman, H. N., & Gaetani, G. F. (2007). Mammalian catalase: A venerable enzyme with new mysteries. *Trends in Biochemical Sciences*, 32(1), 44–50.

Kissa, E. (2001). *Fluorinated Surfactants and Repellents, Second Edition,* CRC Press.

Kottelat, M., & Freyhof, J. (2007). Handbook of European freshwater fishes. *Publications Kottelat*.

Krishnamurthy, P., Wadhwani, A., (2012). Antioxidant Enzymes and Human Health. *Antioxidant enzyme. InTech*.

Kumar, S., Bhardwaj, V. K., Guleria, S., Purohit, R., & Kumar, S. (2022). Improving the catalytic efficiency and dimeric stability of Cu,Zn superoxide dismutase by combining structure-guided consensus approach with site-directed mutagenesis. *Biochimica et Biophysica Acta (BBA) - Bioenergetics*, 1863(1), 148505.

Kwok, K. Y., Yamazaki, E., Yamashita, N., Taniyasu, S., Murphy, M. B., Horii, Y., Petrick, G., Kallerborn, R., Kannan, K., Murano, K., & Lam, P. K. S. (2013). Transport of Perfluoroalkyl substances (PFAS) from an arctic glacier to downstream locations: Implications for sources. *Science of The Total Environment*, 447, 46–55.

Lee, Y. J. (2020). Knockout Mouse Models for Peroxiredoxins. *Antioxidants*, 9(2).

Liguori, I., Russo, G., Curcio, F., Bulli, G., Aran, L., Della-Morte, D., Gargiulo, G., Testa, G., Cacciatore, F., Bonaduce, D., & Abete, P. (2018). Oxidative stress, aging, and diseases. *Clinical Interventions in Aging*, *13*, 757–772.

Lindstrom, A. B., Strynar, M. J., & Libelo, E. L. (2011). Polyfluorinated Compounds: Past, Present, and Future. *Environmental Science & Technology*, *45*(19), 7954–7961.

Margis, R., Dunand, C., Teixeira, F. K., & Margis-Pinheiro, M. (2008). Glutathione peroxidase family – an evolutionary overview. *The FEBS Journal,* 275(15), 3959–3970.

Maté, M. J., Zamocky, M., Nykyri, L. M., Herzog, C., Alzari, P. M., Betzel, C., Koller, F., & Fita, I. (1999). Structure of catalase-A from *Saccharomyces cerevisiae*1. *Journal of Molecular Biology*, *286*(1), 135–149.

McCord, J. M., & Fridovich, I. (1969). Superoxide Dismutase: AN ENZYMIC FUNCTION FOR ERYTHROCUPREIN (HEMOCUPREIN). *Journal of Biological Chemistry*, 244(22), 6049–6055.

Ministero dell'Ambiente e della Tutela del Territorio e del Mare e Istituto di Ricerca sulle Acque – CNR (2013). Realizzazione di uno studio di valutazione del Rischio Ambientale e Sanitario associato alla contaminazione da sostanze perfluoro-alchiliche (PFAS) nel Bacino del Po e nei principali bacini fluviali italiani.

Mureşan, A., Cosgarea, M.; Tomescu, E.; Daicoviciu, D. (2008). The effects of a combination of selenium and vitamin e on cigarette smoke-induced lesions mediated by reactive oxygen species in the rat's larynx. *Veterinary Medicine,* Vol. 65 Issue 1, p65-70.

Nguyen, T. M. H., Bräunig, J., Thompson, K., Thompson, J., Kabiri, S., Navarro, D. A., Kookana, R. S., Grimison, C., Barnes, C. M., Higgins, C. P., McLaughlin, M. J., & Mueller, J. F. (2020). Influences of Chemical Properties, Soil Properties, and Solution pH on Soil–Water Partitioning Coefficients of Per- and Polyfluoroalkyl Substances (PFASs). *Environmental Science & Technology*, 54(24), 15883–15892.

Niu, S., Cao, Y., Chen, R., Bedi, M., Sanders, A. P., Ducatman, A., & Ng, C. (2023). A State-of-the-Science Review of Interactions of Per- and Polyfluoroalkyl Substances (PFAS) with Renal Transporters in Health and Disease: Implications for Population Variability in PFAS Toxicokinetics". *Environmental Health Perspectives*, 131(7), 076002.

Nyeste, K., Dobrocsi, P., Czeglédi, I., Czédli, H., Harangi, S., Baranyai, E., Simon, E., Nagy, S. A., & Antal, L. (2019).
"Age and diet-specific trace element accumulation patterns in different tissues of chub (*Squalius cephalus*): Juveniles are useful bioindicators of recent pollution". *Ecological Indicators*, 101, 1–10.

Organisation for Economic Co-operation and Development [OECD] 2018. Toward a New Comprehensive Global Database of Per- And Polyfluoroalkyl Substances (PFASs): Summary Report on Updating the OECD 2007 List of Per- and Polyfluoroalkyl Substances (PFASs)". *Series on Risk Management* No. 39, ENV/JM/MONO7.

Paul, A. G., Jones, K. C., & Sweetman, A. J. (2009). A First Global Production, Emission, And Environmental Inventory For Perfluorooctane Sulfonate. *Environmental Science & Technology*, *43*(2), 386–392.

Pitter, G., Da Re, F., Canova, C., Barbieri, G., Zare Jeddi, M., Daprà, F., Manea, F., Zolin, R., Bettega, A. M., Stopazzolo, G., Vittorii, S., Zambelli, L., Martuzzi, M., Mantoan, D., & Russo, F. (2020).
Serum Levels of Perfluoroalkyl Substances (PFAS) in Adolescents and Young Adults Exposed to Contaminated Drinking Water in the Veneto Region, Italy: A Cross-Sectional Study Based on a Health Surveillance Program. *Environmental Health Perspectives*, 128(2), 027007.

Piva, E., Schumann, S., Dotteschini, S., Brocca, G., Radaelli, G., Marion, A., Irato, P., Bertotto, D., & Santovito, G. (2022). Antioxidant Responses Induced by PFAS Exposure in Freshwater Fish in the Veneto Region. *Antioxidants*, *11*(6), Articolo 6.

Poli, A., Fabbri, E., Agnisola, C., Calamita, G., Santovito, G., & Verri, T. (2018). Fisiologia animale. EdiSES.

Prevedouros, K., Cousins, I. T., Buck, R. C., & Korzeniowski, S. H. (2006). Sources, Fate and Transport of Perfluorocarboxylates. *Environmental Science & Technology*, *40*(1), 32–44.

Protter, D. S. W., & Parker, R. (2016). Principles and Properties of Stress Granules. *Trends in Cell Biology*, *26*(9), 668–679.

Rempel, A., Gutkoski, J. P., Nazari, M. T., Biolchi, G. N., Cavanhi, V. A. F., Treichel, H., & Colla, L. M. (2021). Current advances in microalgae-based bioremediation and other technologies for emerging contaminants treatment. *Science of The Total Environment*, *772*, 144918.

Rhee, S. G. (2016). Overview on Peroxiredoxin. *Molecules and Cells*, 39(1), 1–5.

Russell, M. H., Berti, W. R., Szostek, B., & Buck, R. C. (2008). Investigation of the Biodegradation Potential of a Fluoroacrylate Polymer Product in Aerobic Soils. *Environmental Science & Technology*, 42(3), 800–807.

Santovito, G., Piccinni, E., Cassini, A., Irato, P., & Albergoni, V. (2005). Antioxidant responses of the Mediterranean mussel, *Mytilus galloprovincialis*, to environmental variability of dissolved oxygen.

Comparative Biochemistry and Physiology Part C: Toxicology & Pharmacology, 140(3), 321–329.

Savoca, D., & Pace, A. (2021). Bioaccumulation, Biodistribution, Toxicology and Biomonitoring of Organofluorine Compounds in Aquatic Organisms. *International Journal of Molecular Sciences*, 22(12), Articolo 12.

Schultz, M. M., Barofsky, D. F., & Field, J. A. (2003). Fluorinated Alkyl Surfactants. *Environmental Engineering Science*, *20*(5), 487–501.

Shi, G., Xie, Y., Guo, Y., & Dai, J. (2018). 6:2 fluorotelomer sulfonamide alkylbetaine (6:2 FTAB), a novel perfluorooctane sulfonate alternative, induced developmental toxicity in zebrafish embryos. *Aquatic Toxicology*, 195, 24–32.

Shi, X., Du, Y., Lam, P. K. S., Wu, R. S. S., & Zhou, B. (2008). Developmental toxicity and alteration of gene expression in zebrafish embryos exposed to PFOS. *Toxicology and Applied Pharmacology*, 230(1), 23–32.

Sikora, A., Michalski, R., Mesjasz, A., Hardy, M., Ouari, O., Zielonka, J., & Kalyanaraman, B. (2017). 77—N,N,N,N-tetramethylhydroethidine (TMHE)—In search for Novel Probes for the Detection of Superoxide Radical Anion. *Free Radical Biology and Medicine*, 112, 64.

Srivastava, S. K., & Ansari, N. H. (1980). The peroxidatic and catalatic activity of catalase in normal and acatalasemic mouse liver. *Biochimica et Biophysica Acta (BBA) - General Subjects*, *633*(3), 317–322.

Stephenie, S., Chang, Y. P., Gnanasekaran, A., Esa, N. M., & Gnanaraj, C. (2020). An insight on superoxide dismutase (SOD) from plants for mammalian health enhancement. *Journal of Functional Foods*, *68*, 103917.

Thomaidis, N. S., Asimakopoulos, A. G., & Bletsou, A. A. (2012). Emerging contaminants: a tutorial mini-review. *Global NEST Journal*, Vol 14, No 1, pp 72-79.

Tolomeo, A. M., Carraro, A., Bakiu, R., Toppo, S., Garofalo, F., Pellegrino, D., Gerdol, M., Ferro, D., Place, S. P., & Santovito, G. (2019). Molecular characterization of novel mitochondrial peroxiredoxins from the Antarctic emerald rockcod and their gene expression in response to environmental warming. *Comparative Biochemistry and Physiology Part C: Toxicology & Pharmacology*, *225*, 108580.

Tolomeo, A. M., Carraro, A., Bakiu, R., Toppo, S., Place, S. P., Ferro, D., & Santovito, G. (2016). Peroxiredoxin 6 from the Antarctic emerald rockcod: Molecular characterization of its response to warming. *Journal of Comparative Physiology B*, *186*(1), 59–71.

Tromba C. (2017). Inquinamento da PFAS in Veneto. Dopo gli USA tocca all'Italia. *Epidemiol Prev*, 41, pp. 232-236.

Ulhaq, M., Sundström, M., Larsson, P., Gabrielsson, J., Bergman, Å., Norrgren, L., & Örn, S. (2015). Tissue uptake, distribution and elimination of 14C-PFOA in zebrafish *(Danio rerio). Aquatic Toxicology*, 163, 148–157.

Valero, Y., Martínez-Morcillo, F. J., Esteban, M. Á., Chaves-Pozo, E., & Cuesta, A. (2015). Fish Peroxiredoxins and Their Role in Immunity. *Biology*, *4*(4), Articolo 4.

Valko, M., Izakovic, M., Mazur, M., Rhodes, C. J., & Telser, J. (2004). Role of oxygen radicals in DNA damage and cancer incidence. *Molecular and Cellular Biochemistry*, 266(1), 37–56.

Valko, M., Morris, H., Mazúr, M., Rapta, P., & Bilton, R. F. (2001). Oxygen free radical generating mechanisms in the colon: Do the semiquinones of vitamin K play a role in the aetiology of colon cancer? *Biochimica et Biophysica Acta (BBA) - General Subjects*, 1527(3), 161–166.

van Asselt, E. D., Rietra, R. P. J. J., Römkens, P. F. A. M., & van der Fels-Klerx, H. J. (2011). Perfluorooctane sulphonate (PFOS) throughout the food production chain. *Food Chemistry*, 128(1), 1–6.

Wen, W., Xia, X., Zhou, D., Wang, H., Zhai, Y., Lin, H., Chen, J., & Hu, D. (2019). Bioconcentration and tissue distribution of shorter and longer chain perfluoroalkyl acids (PFAAs) in zebrafish (*Danio rerio*): Effects of perfluorinated carbon chain length and zebrafish protein content. *Environmental Pollution*, 249, 277–285.

Wilhelm Filho D. (2007). Reactive oxygen species, antioxidants and fish mitochondria. *Frontiers in Bioscience,* 12, 1229-1237.

Williams, M. D., Remmen, H. V., Conrad, C. C., Huang, T. T., Epstein, C. J., & Richardson, A. (1998). Increased Oxidative Damage Is Correlated to Altered Mitochondrial Function in Heterozygous Manganese Superoxide Dismutase Knockout Mice*. *Journal of Biological Chemistry*, 273(43), 28510–28515.

Witko-Sarsat, V., Gausson, V., Nguyen, A.-T., Touam, M., Drüeke, T., Santangelo, F., & Descamps-Latscha, B. (2003). AOPP-induced activation of human neutrophil and monocyte oxidative metabolism: A potential target for N-acetylcysteine treatment in dialysis patients. *Kidney International*, 64(1), 82–91.

Wolf, J. C., & Wolfe, M. J. (2005). A Brief Overview of Nonneoplastic Hepatic Toxicity in Fish. *Toxicologic Pathology*, *33*(1), 75–85.

Wolozin, B., & Ivanov, P. (2019). Stress granules and neurodegeneration. *Nature Reviews Neuroscience*, *20*(11), Articolo 11.

Yamada, S., & Guo, X. (2018). Peroxiredoxin 4 (PRDX4): Its critical in vivo roles in animal models of metabolic syndrome ranging from atherosclerosis to nonalcoholic fatty liver disease. *Pathology International*, *68*(2), 91–101.

Yamashita, N., Taniyasu, S., Petrick, G., Wei, S., Gamo, T., Lam, P. K. S., & Kannan, K. (2008). Perfluorinated acids as novel chemical tracers of global circulation of ocean waters. *Chemosphere*, 70(7), 1247–1255.

Zámocký, M., & Koller, F. (1999).
Understanding the structure and function of catalases: Clues from molecular evolution and in vitro mutagenesis. *Progress in Biophysics and Molecular Biology*, 72(1), 19–66.

Zhang, Y.-G., Wang, L., Kaifu, T., Li, J., Li, X., & Li, L. (2016). Featured Article: Accelerated decline of physical strength in peroxiredoxin-3 knockout mice. *Experimental Biology and Medicine*, 241(13), 1395–1400.